iScience

Article

The noncoding circular RNA *circHomer1* regulates synaptic development and experience-dependent plasticity in the mouse visual cortex

Graphical abstract

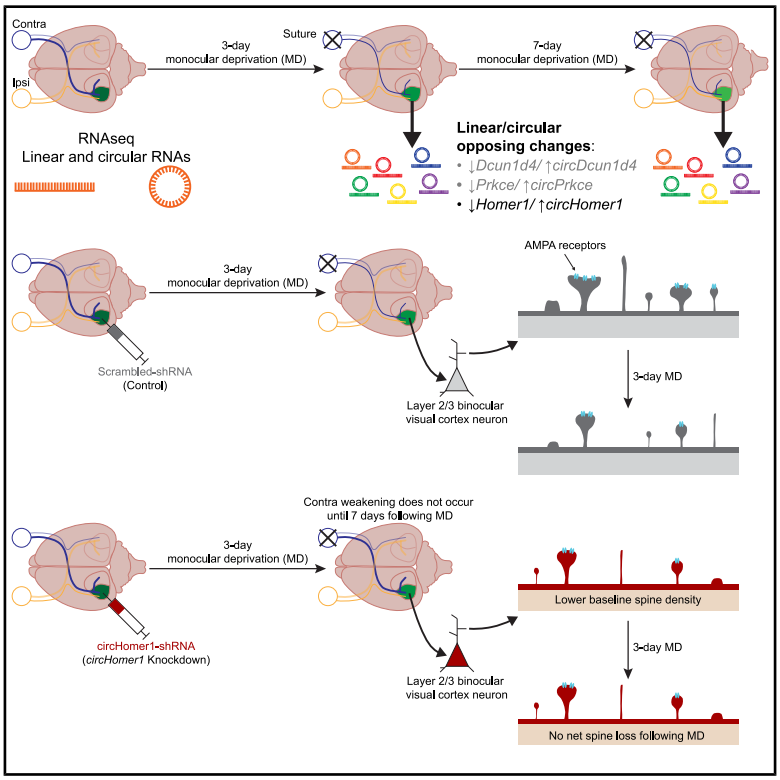

Highlights

- Screen for experience-dependent circular RNAs using monocular deprivation in mice
- The circular RNA, *circHomer1*, is upregulated after 3 days of monocular deprivation
- *circHomer1*-depletion delays closed eye depression following monocular deprivation
- *circHomer1* regulates developmental dendritic spine density and plasticity

Authors

Kyle R. Jenks, Ying Cai, Marvin Eduarte Nayan, ..., Nikolaos Mellios, Mriganka Sur, Jacque Pak Kan Ip

Correspondence

msur@mit.edu (M.S.), jacqueip@cuhk.edu.hk (J.P.K.I.)

In brief

Genetics; Molecular biology; Neuroscience; Developmental biology

Jenks et al., 2025, iScience *28*, 113421
September 19, 2025
https://doi.org/10.1016/j.isci.2025.113421

CellPress

iScience

CellPress
OPEN ACCESS

Article

The noncoding circular RNA *circHomer1* regulates synaptic development and experience-dependent plasticity in the mouse visual cortex

Kyle R. Jenks,[1,10] Ying Cai,[2,10] Marvin Eduarte Nayan,[3,10] Katya Tsimring,[1] Keji Li,[1,4] José C. Zepeda,[1] Gregg R. Heller,[1] Chloe Delepine,[1] Jennifer Shih,[1] Shiyang Yuan,[2] Yao Zhu,[2] Ye Wang,[5] Yangyang Duan,[5] Amy K.Y. Fu,[5] Taeyun Ku,[6] Dae Hee Yun,[1] Kwanghun Chung,[1] Nikolaos Mellios,[7,8] Mriganka Sur,[1,*] and Jacque Pak Kan Ip[2,9,11,*]

[1]Department of Brain and Cognitive Sciences, The Picower Institute for Learning and Memory, Massachusetts Institute of Technology, Cambridge, MA 02139, USA
[2]School of Biomedical Sciences, The Chinese University of Hong Kong, Hong Kong, China
[3]Department of Biology, Massachusetts Institute of Technology, Cambridge, MA 02139, USA
[4]Department of Radiology, Massachusetts General Hospital, Harvard Medical School, Boston, MA 02114, USA
[5]Division of Life Science, The Hong Kong University of Science and Technology, Clear Water Bay, Hong Kong, China
[6]Graduate School of Medical Science and Engineering, Korea Advanced Institute of Science and Technology, Daejeon, Korea
[7]Circular Genomics Inc, San Diego, CA 92121, USA
[8]Previously at: University of New Mexico, Department of Neurosciences, Albuquerque, NM 87131, USA
[9]Gerald Choa Neuroscience Institute, The Chinese University of Hong Kong, Hong Kong, China
[10]These authors contributed equally
[11]Lead contact
*Correspondence: msur@mit.edu (M.S.), jacqueip@cuhk.edu.hk (J.P.K.I.)
https://doi.org/10.1016/j.isci.2025.113421

SUMMARY

Circular RNAs (circRNAs) are closed-loop, single-stranded RNAs particularly enriched in the brain. Despite this enrichment, and evidence showing that synaptic development and plasticity alter their expression *in vitro*, circRNA regulation by and function in experience-dependent plasticity *in vivo* remain unexplored. Through transcriptome-wide analysis in juvenile mouse primary visual cortex (V1) following monocular deprivation (MD), we identified that the circular and the activity-dependent mRNA forms of the *Homer1* gene, *circHomer1* and *Homer1a,* respectively, showed opposing changes in expression following 3-day MD: *circHomer1* increased while *Homer1a* decreased. Knockdown of *circHomer1* delayed the depression of closed-eye responses normally observed after 3-day MD. *circHomer1*-knockdown reduced average dendritic spine size prior to MD but also blocked further MD-induced shrinkage, consistent with impaired structural plasticity. *circHomer1*-knockdown also prevented the reduction of surface AMPA receptors normally observed after 3-day MD. Our findings highlight the essential role of *circHomer1* in V1 synaptic development and experience-dependent plasticity.

INTRODUCTION

Experience-dependent plasticity is a tightly regulated process that requires orchestrated gene transcription to form mRNAs that are subsequently translocated and translated into proteins to induce the functional and structural reorganization of synapses.[1] Though we now know a great deal about the mRNAs recruited by and required for experience-dependent plasticity, it remains unclear if other forms of non-coding/coding RNAs are as tightly regulated as their mRNA counterparts and if they contribute to experience-dependent plasticity.[2,3] Recent RNA-sequencing screens have shown that a plethora of genes that produce alternatively spliced mRNAs also generate close-looped isoforms composed of backspliced and covalently joined exons and/or introns known as circular RNAs (circRNAs).[4] Although much is still unknown about the precise mechanisms that govern the biogenesis, regulation, and function of circRNAs; there is emerging evidence that circRNAs may have important roles in the brain.[3,5] They are dynamically expressed during brain development, are localized to synapses,[6] and a small number of circRNAs have been shown to affect neuronal gene expression, miRNA availability, and regulate behavior.[7–9] However, it remains unclear how many circRNAs might play a role in regulating experience-dependent plasticity, highlighting the need for screens to identify putative candidates.

Ocular dominance plasticity in mouse binocular primary visual cortex (V1) is a well-defined model of cortical plasticity induced by monocular deprivation (MD), typically via suture of the eyelids, during a developmental critical period.[10–15] During this window, which in mice begins at postnatal day (P)21 and ends around P35,[16] MD induces a reduction of V1 responses to the deprived eye after ~3 days of deprivation, followed by an

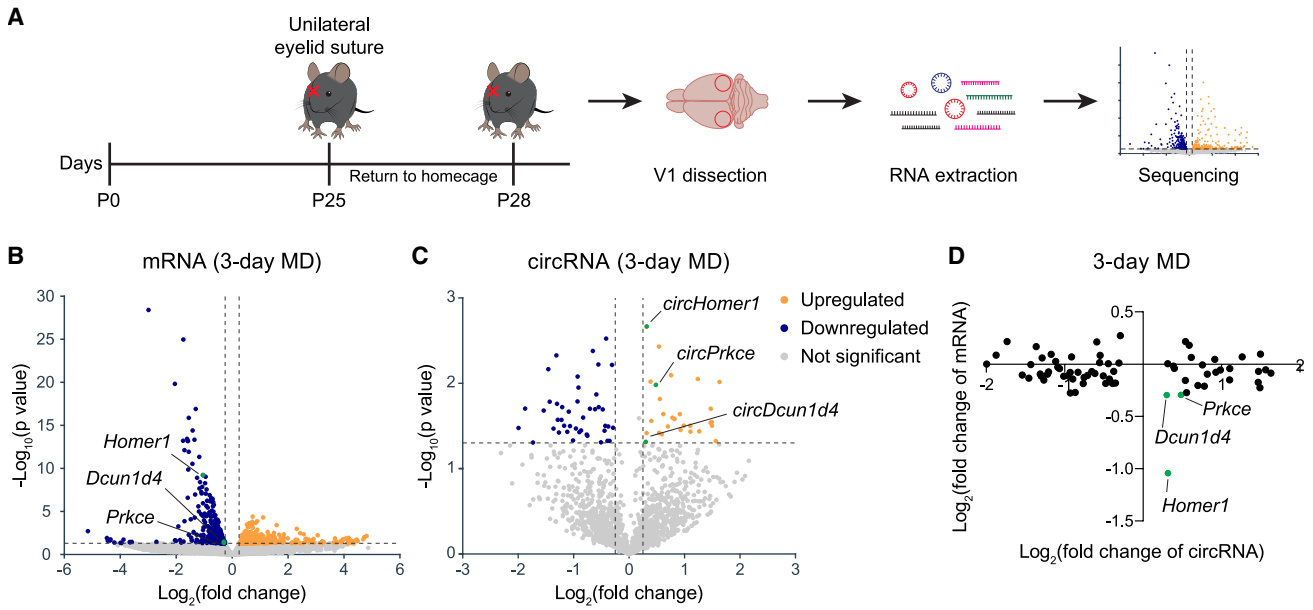

Figure 1. Experience-dependent circRNAs in V1 identified through MD

(A) Timeline and schematic of 3-day MD RNAseq screen.

(B) Volcano plot of the mRNA sequencing of V1 after 3-day MD (n = 3 mice per group).

(C) Volcano plot of the circRNA sequencing of V1 after 3-day MD (n = 3 mice per group). The ipsilateral hemisphere (ipsi) served as a control for MD induced changes in the contralateral hemisphere (contra) for both mRNA and circRNA expression.

(D) Fold change of differentially expressed circRNAs and their mRNA isoforms after 3-day MD. The mouse and brain silhouette were adapted from https://doi.org/10.5281/zenodo.8044766 and https://doi.org/10.5281/zenodo.3925971. The datapoints in green indicate *circHomer1*, *circPrkce*, and *circDcun1d4*, whose circular and linear isoforms exhibit a change in the opposite direction after 3-day MD.

increase of responses to the non-deprived eye[17] after ~7 days of deprivation.[11,13–15,18–20] MD also leads to the activity-dependent up- and down-regulation of many mRNAs known to regulate synaptic plasticity.[10–15] We have successfully used MD in the past to screen for and identify miRNAs, another unique class of RNA species, regulated by and critical for experience-dependent plasticity.[2] Thus, we sought to similarly use MD to identify circRNAs in mouse V1 that could be involved in regulating experience-dependent plasticity and synaptic function.

By screening for differentially expressed mRNAs and circRNAs in the developing mouse V1 following 3 days of MD (3-day MD), we discovered multiple circRNAs whose expression was regulated by experience-dependent plasticity. We further explored the role of the circRNA *circHomer1* in experience-dependent plasticity, as the expression of *circHomer1* was opposite that of its linear, activity-dependent form *Homer1a* and *circHomer1* has previously been shown to be localized to synapses and involved in cognitive flexibility and reversal learning.[9,21,22] Using *circHomer1*-specific knockdown in V1, we showed that *circHomer1* knockdown delays normal closed-eye response depression following 3-day MD. While *circHomer1* knockdown alone decreases the average size of dendritic spines on layer 2/3 neurons, it also prevents the decrease in spine size following 3-day MD. Knockdown of *circHomer1* also impaired the downregulation of the AMPA receptor subunit GluA1 following 3-day MD. Together, these data provide the first evidence of an experience-dependent circRNA that is required for normal synaptic development and experience-dependent plasticity induced by short-term MD.

RESULTS

Circular RNA expression is regulated by experience-dependent plasticity

To identify potential experience-regulated circRNAs, we performed MD in mice beginning at P25, collected tissue from V1 and examined the transcriptomic profile after 3-day MD (Figure 1A). We normalized RNA expression in the hemisphere contralateral to the deprived eye, where the majority of change in synaptic drive occurs, to expression in the ipsilateral hemisphere (within-subject) which receives significantly less input from the deprived eye and has significantly less change in gene expression.[2] Before exploring the circRNA expression profile, we first examined the mRNA expression profile to validate our results against previously observed mRNA regulation by MD. We identified a total of 1173 differentially expressed mRNAs, with more mRNAs downregulated than upregulated (472 upregulated and 701 downregulated, Figure 1B). mRNAs known to be downregulated during MD, such as *Bdnf* and *Nptx2*,[23] were also downregulated in our data (Table S1). Having confirmed that our preparation replicated the known regulation of mRNA expression by 3-day MD,[24] we next examined the regulation of circRNAs. We used a published circRNA alignment tool, circtools, to detect circRNA transcripts by virtue of their unique out-of-order junctional reads.[23] A total of 1489 unique circRNAs were detected, with 73 differentially expressed (Figure 1C; Table S1). Of the differentially expressed circRNAs, we observed 27 significantly upregulated circRNAs and 46 downregulated

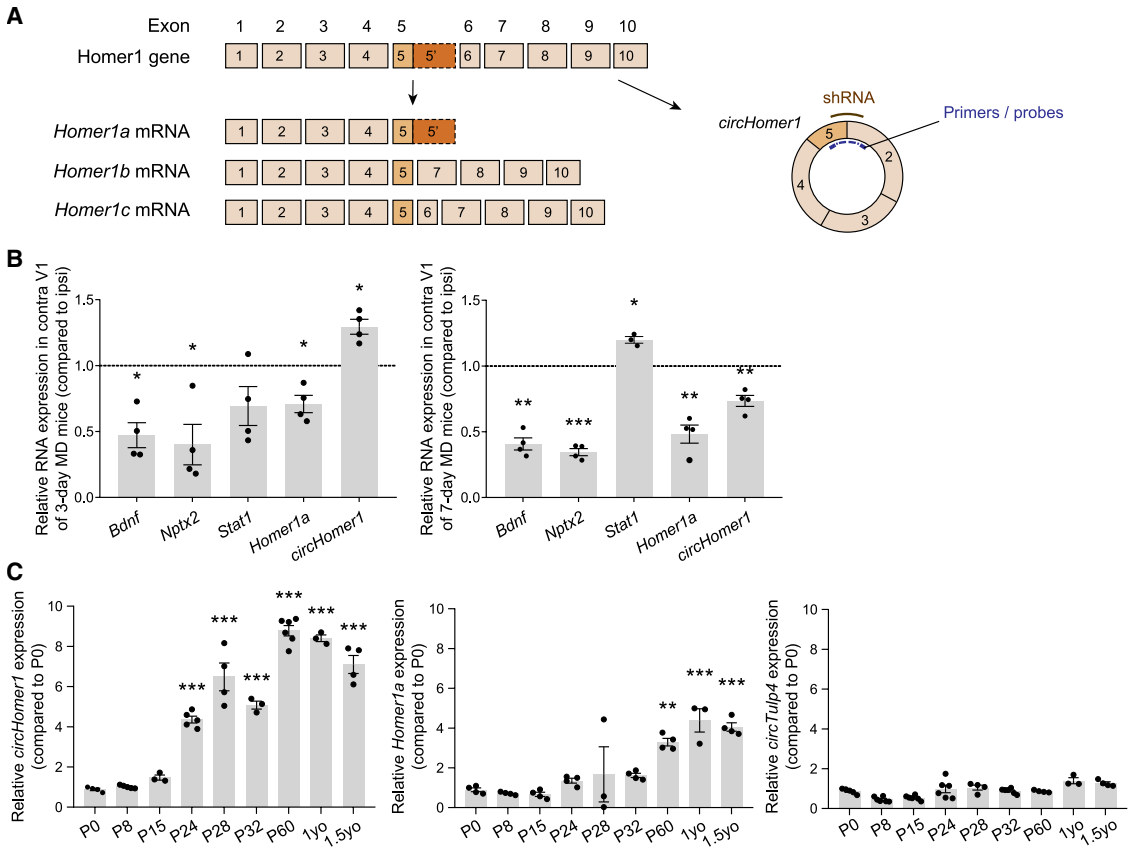

Figure 2. *circHomer1* expression is regulated by experience-dependent plasticity and upregulated during the ocular dominance critical period

(A) The mouse Homer1 gene encodes long and short versions of the synaptic protein Homer1 and a noncoding circRNA, *circHomer1*.

(B) RT-qPCR quantification of selected mRNAs and *circHomer1* after 3-day (left) or 7-day (right) MD in contralateral V1 relative to ipsilateral V1 (n = 3–4 mice per group, one sample t-test).

(C) *circHomer1* (left), *Homer1a* (middle), and *circTulp4* (right) expression measured by RT-qPCR at several timepoints in mouse V1 across development and into adulthood (n = 3–6 mice per group, one-way ANOVA following Tukey multiple comparisons). Yo, years old.

Data are presented as mean ± SEM. *p < 0.05, **p < 0.01, ***p < 0.001.

circRNAs. Some of the genes from which these differentially expressed circRNAs were derived have known roles in synaptic plasticity and function (Figure S1A). Indeed, we also identified changes in the corresponding mRNA isoforms of several differentially expressed circRNAs. Of these, the linear isoforms of *circHomer1*, *circPrkce*, and *circDcun1d4* were of interest as they exhibited changes in the opposite direction compared to their circular counterparts, suggesting their circRNA expression was regulated by experience independently of the overall gene transcription rate (Figure 1D). We also performed a transcriptomic analysis of mRNAs and circRNAs in V1 after 7-day MD (Figures S1B–S1E; Table S2). *circPrkce*, *circDcun1d4*, and their linear isoforms were not differentially expressed at this timepoint, while linear *Homer1a* remained downregulated and *circHomer1* was no longer upregulated. Based on these findings, and the known role of *Homer1a* in synaptic plasticity, we chose to more closely examine the experience-dependent and developmental regulation and role of *circHomer1* in mouse V1.

circHomer1 expression is developmentally regulated

circHomer1 is composed of exons 2 through 5 of the *Homer1* gene, with backsplicing between exon 2 and 5 (Figure 2A). Using primers targeting the backsplice junction of *circHomer1*, we next sought to validate the observed changes in contralateral V1 *circHomer1* expression, relative to ipsilateral V1, after 3-day and 7-day MD using RT-qPCR (Figure 2B). In addition, we examined several mRNAs known to be regulated by MD. As expected after 3-day MD, *Bdnf* and *Nptx2* mRNA were downregulated in contralateral V1[24]. *Homer1a* mRNA was also significantly downregulated after 3-day MD, in contrast to *circHomer1*, validating the dissociation between *Homer1a* and *circHomer1* expression after 3-day MD (Figure 2B, left). After 7-day MD, *Stat1*,[25] a regulator of homeostatic synaptic plasticity, was upregulated in contralateral V1 (Figure 2B, right) as previously shown for prolonged MD.[17,24,25] We also saw that the expression of *circHomer1* was significantly decreased after 7-day MD, along with *Homer1a* (Figure 2B, right). These results validate the RNA-seq data showing that experience-dependent regulation of

circHomer1 expression is distinct at 3-day MD from that of its linear experience-dependent counterpart *Homer1a*.

The expression of many mRNAs required for normal, developmental experience-dependent plasticity peaks during the critical period. To determine the developmental expression profiles of *Homer1a* and *circHomer1* over the mouse's lifespan, we measured their expression in V1 at various time points relative to P0 using RT-qPCR. *circHomer1* expression increased significantly starting at ~ P24, aligning to the start of the critical period (Figure 2C, left), while *Homer1a* expression did not increase significantly until P60, past the close of the critical period (Figure 2C, middle). *circHomer1* expression appeared to plateau at P60 and remained at similar levels of expression in mice as old as 1.5 years. The expression of another circRNA, *circTulp4*, did not change across development or adulthood, indicating that the developmental expression profile of *circHomer1* is not a shared feature of all circRNAs (Figure 2C, right).

circHomer1-depletion delays ocular dominance plasticity

The regulation of *circHomer1* expression by MD and the peak in *circHomer1* expression at the start of the critical period mirrors that of linear mRNAs with known roles in ocular dominance plasticity. To determine if *circHomer1* is required for ocular dominance plasticity following MD, we used a short hairpin RNA (shRNA)-mediated depletion strategy targeting the backsplice junction of *circHomer1*, which has been previously validated *in vivo* to specifically downregulate *circHomer1*, and not linear *Homer1* mRNAs (including *Homer1a*, *Homer1b*, and *Homer1c*),[9] in the cortex. We re-confirmed the specificity of knockdown using adeno-associated viruses (AAV)-mediated transduction of the shRNA in mouse V1, which resulted in a significant reduction of *circHomer1* RNA with no changes in *Homer1a*, *Homer1b*, or *Homer1c* mRNA expression (Figure 3A). sh-circHomer1 also had no effect on total Homer1 protein levels (Figure 3B).

To examine the effects of *circHomer1* depletion on ocular dominance plasticity, we quantified eye-specific responses in the binocular zone of V1 by using the optical imaging of intrinsic hemodynamic signals measured before and after 3-day or 7-day MD (Figure 3C). We then compared results between mice injected with a sh-scramble (control) or sh-circHomer1 virus (Figure 3D). To compare the relative strength of visual input from the two eyes in V1, the normalized difference between the contralateral (dominant-eye) and ipsilateral responses measured during optical imaging was calculated to determine the ocular dominance index (ODI). Change in ODI following 3-day or 7-day MD of the contralateral eye was then used as a measure of experience-dependent plasticity.[26]

Prior to MD (preMD), there was no difference in baseline ODI between sh-scramble and sh-circHomer1 mice, with responses biased toward the dominant, contralateral eye (Figure 3E). After 3-day MD, the ODI of sh-scramble mice decreased significantly (shifted toward the open, ipsilateral eye) as expected.[24,27,28] In contrast, the ODI of sh-circHomer1 mice was unchanged after 3-day MD (Figure 3E). After 7-day MD, however, the ODI of sh-circHomer1 mice was significantly decreased and no longer significantly different than that of sh-scramble mice (Figure 3E).

The ODI shifts at 3-day and 7-day MD are driven by an initial decrease in contralateral drive and delayed increase in ipsilateral drive, respectively.[24,27,28] To see if both these eye-specific changes instead occurred between 3-day and 7-day MD in sh-circHomer1 mice, we examined the responses driven by the contralateral and ipsilateral eyes separately (Figure 3F). Unlike in the sh-scramble mice, and as expected from the lack of change in ODI, contralateral closed-eye responses of sh-circHomer1 mice did not decrease after 3-day MD (Figure 3F, left). Similarly, ipsilateral open-eye responses were already significantly increased in sh-scramble mice after 3-day MD, whereas they were paradoxically reduced in sh-circHomer1 mice (Figure 3F, right). Despite the differences in eye-specific changes after 3-day MD, however, by 7-day MD, both contralateral and ipsilateral responses in the sh-circHomer1 mice were comparable to the sh-scramble mice (Figure 3F). Thus, *circHomer1* depletion does not grossly impair the eye-specific development of contralateral and ipsilateral visual drive and delays, but does not block, the expression of experience-dependent ocular dominance plasticity following MD.

circHomer1 regulates dendritic spine morphology and surface AMPA receptor trafficking

MD induces the rapid remodeling of the dendritic spines of mouse layer 2/3 V1 neurons, with 3-day MD significantly decreasing average spine volumes.[10] As we had found that the depletion of *circHomer1* blocked the depression of closed eye responses at 3-day MD (Figure 3), we hypothesized that the depletion of *circHomer1* would likewise impair 3-day MD-induced spine shrinkage. We injected an AAV expressing RFP and either sh-circHomer1 or sh-scramble shRNA into the binocular region of V1 at P15, prior to the start of the critical period. We also injected AAV9-hSyn-DIO-EGFP (structural marker) and AAV9-CaMKIIa-Cre virus to sparsely label neurons and quantified spine morphology of labeled layer 2/3 V1 neurons from mice that had undergone no MD (No MD), 3-day MD, or 7-day MD. To achieve a more detailed analysis of the dendritic spine structure than is possible with traditional confocal imaging, we used epitope-preserving magnified analysis of the proteome (eMAP) to expand our tissue samples (Figure 4A). The apical dendrites of V1 layer 2/3 pyramidal neurons expressing both GFP and RFP were selected for further analysis (Figure 4B, left). Based on their morphology, dendritic spines were classified into four categories: mushroom, stubby, thin, and filopodia using standard criteria (Figures 4B and 4C).[29]

In No MD mice, sh-circHomer1 led to a significant drop in the density and percentage of mature mushroom spines,[30] but not immature spines (stubby, thin, and filopodia)[30] (Figures 4D and 4E). This baseline effect was surprising given the normal baseline ODI and eye-specific responses we had observed in preMD sh-circHomer1 mice. After 3-day MD in sh-scramble mice, as expected, there was a significant decrease in the density and percentage of mature mushroom spines when compared to the No MD condition. Conversely, the density of both mature and immature spines remained unchanged after 3-day MD in the sh-circHomer1 mice. After 7-day MD, in the sh-scramble mice, the density and percentage of mature spines remained lower compared to the No MD condition, while the density of

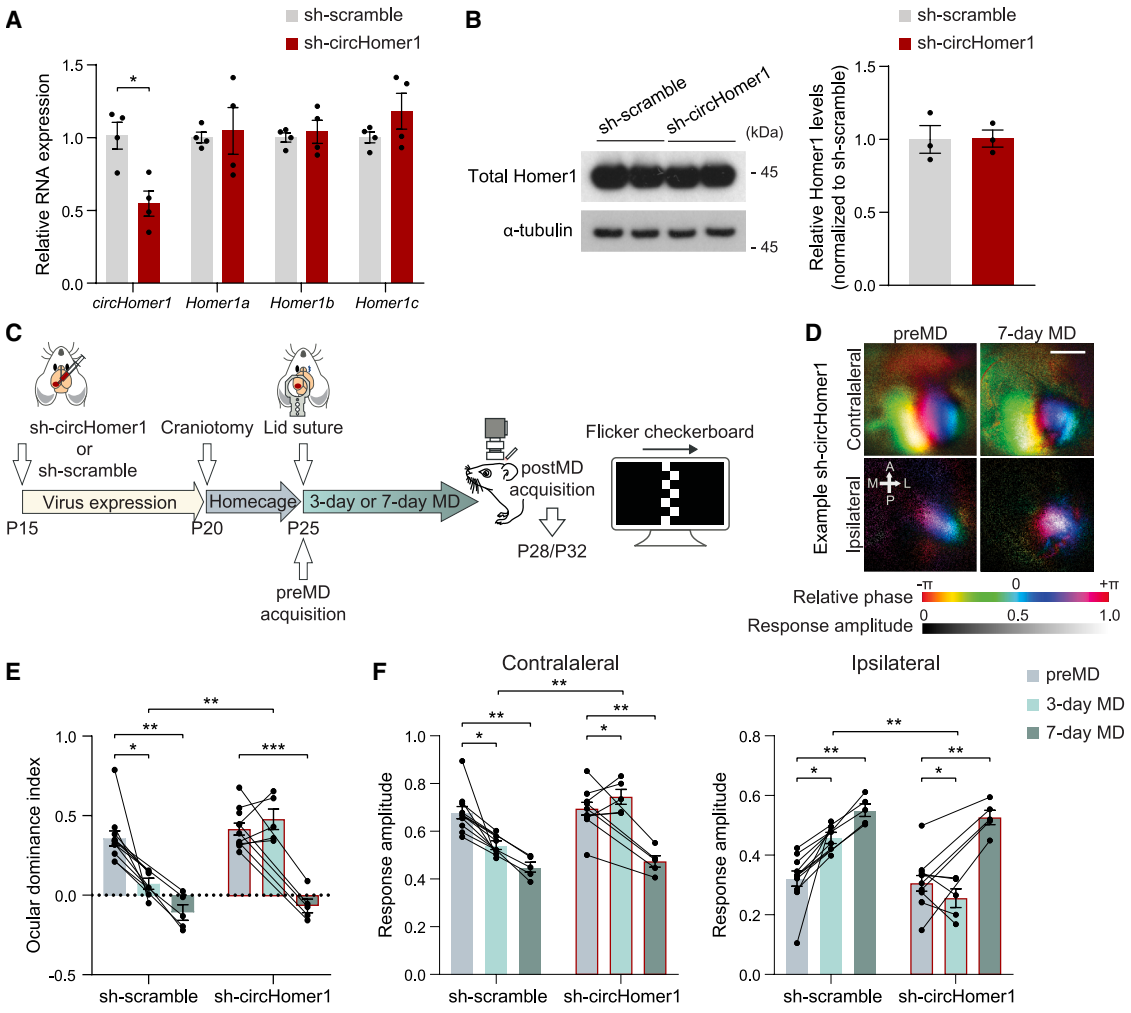

Figure 3. *circHomer1* depletion delays the expression of ocular dominance plasticity in V1 following MD

(A) sh-circHomer1 specifically reduces the expression of *circHomer1,* but not linear *Homer1,* in mouse V1 (n = 4 mice per group, Student's t test).

(B) sh-circHomer1 has no effect on total Homer1 protein levels as measured by Western blot (n = 3 mice per group).

(C) Mice were injected with either sh-circHomer1 or sh-scramble virus at P15, a craniotomy was performed at P22 to implant a cranial window, then a preMD optical imaging session was done, and the contralateral eye-lid sutured at P25. After either 3-day or 7-day MD, the eyelid was reopened, and post-MD imaging done.

(D) Example retinotopic maps from a sh-circHomer1 mouse, obtained with optical imaging. The color corresponds with different phases of the visual stimulus (consistent with the visual field map) and brightness shows the amplitude of the cortical response. Top, contralateral-eye responses, preMD (left) and after 7-day MD (right). Bottom, ipsilateral-eye responses. Scale bar = 500 μm

(E) Ocular dominance index (ODI) changes after 3-day or 7-day MD for mice injected with sh-scramble or sh-circHomer1 virus. Each dot shows the average ODI for one animal, and gray lines show the change of ODI for one animal (n = 5–11 mice per group, mixed-effects model following Holm-Sidak multiple comparisons test).

(F) Normalized response amplitudes driven by the contralateral (left) and ipsilateral (right) eyes (n = 5–11 mice per group, mixed-effects model following Holm-Sidak multiple comparisons test).

Data are presented as mean ± SEM. *p < 0.05; **p < 0.01; ***p < 0.001.

immature spines showed a significant increase. Mature and immature spine density in sh-circHomer1 mice after 7-day MD again remained unchanged compared to the No MD condition, but was no longer significantly different than the sh-scramble mice (Figures 4D and 4E).

As categorical classification could obscure more subtle changes in the dendritic spines of sh-circHomer1 neurons, we also analyzed the average spine volume by performing 3D reconstruction. *circHomer1* depletion led to a more than 50% decrease in average spine volume in the No MD condition (Figure 4F). After 3-day MD, the average spine volume decreased by more than 70% in sh-scramble mice compared to the No MD condition. In contrast, 3-day MD did not significantly alter spine volume in sh-circHomer1 mice (Figures 4F and 4G). After 7-day MD, spine volume was still significantly decreased in sh-scramble mice compared to the No MD

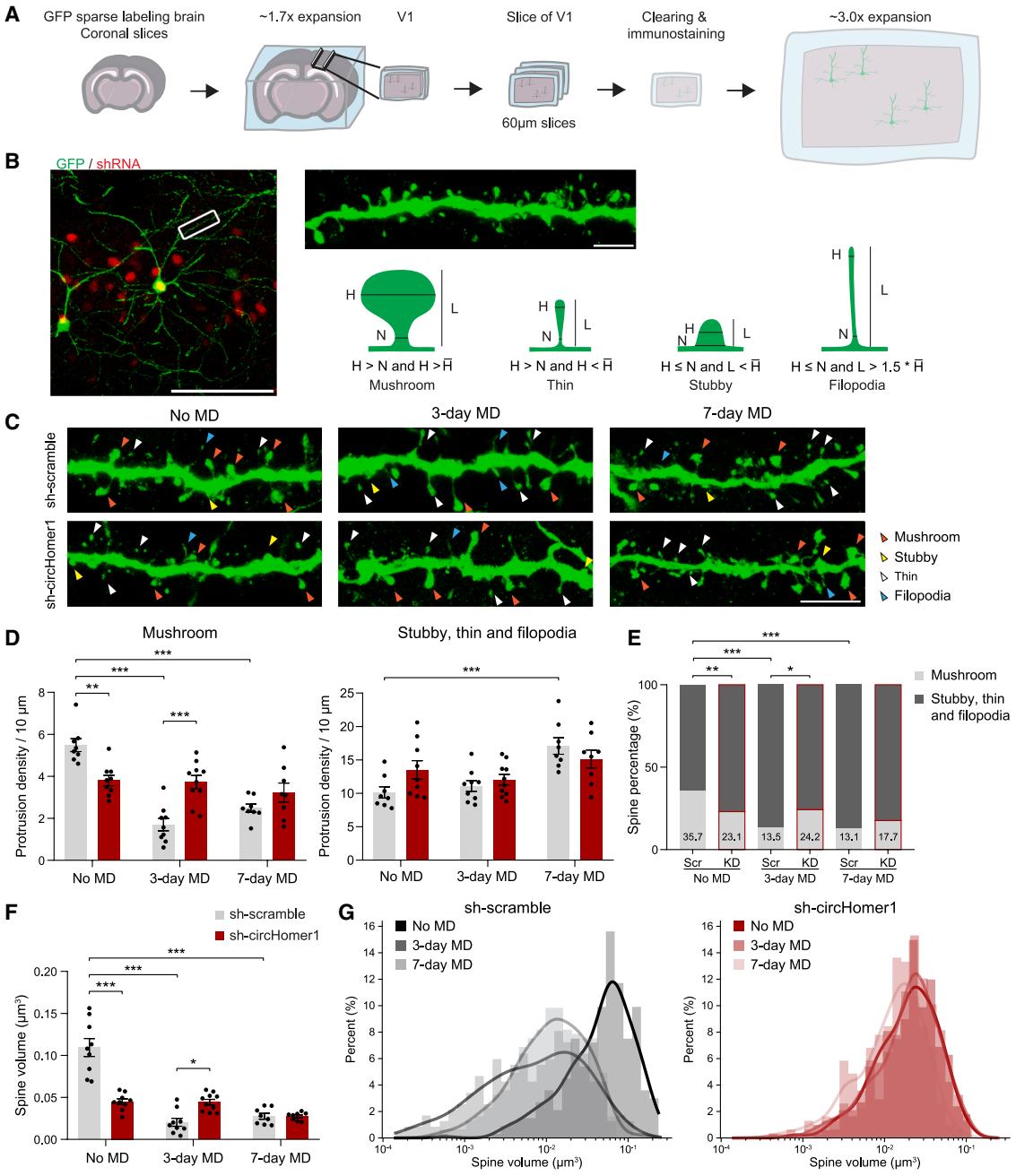

Figure 4. Depletion of *circHomer1* affects spine morphology of V1 neurons

(A) A schematic of tissue preparation and eMAP.

(B) Neurons expressing both GFP and RFP (denoting shRNA) were selected for analysis (left). Dendritic spines were classified into four categories based on their morphology (right). Scale bars = 100 μm (left, estimated to be 33.33 μm prior to 3× expansion), and 10 μm (right, estimated to be 3.33 μm prior to 3× expansion). H, head width; N, neck width; L, length; $\overline{H}$, average head width in the No MD sh-scramble group.

(C) Representative images showing apical dendrites of layer 2/3 neurons in V1 in the No MD, 3-day MD, and 7-day MD condition from the sh-scramble (top) or sh-circHomer1 (bottom) group. Arrows indicate different types of dendritic spines. Scale bar = 10 μm (estimated to be 3.33 μm prior to 3× expansion).

(D) Density of mushroom spines, and immature spines (stubby spines, thin spines and filopodia) on apical dendrites of layer 2/3 neurons in V1 in the No MD, 3-day MD, and 7-day MD condition from the sh-scramble (gray) or sh-circHomer1 (pink) group (n = 8–10 dendrites from 3 mice per group, values were normalized to 3× expansion factor, two-way ANOVA following Tukey multiple comparisons).

(E) Spine morphology types as a percentage of total spines. The percentage of mushroom spines is labeled on the bar.

(legend continued on next page)

condition, and while the sh-circHomer1 spine volume remained unchanged, the sh-scramble and sh-circHomer1 spine volumes were not significantly different at 7-day MD (Figure 4F). Taken together, our findings suggest that *circHomer1* plays a crucial role in regulating the structural morphology of dendritic spines both during normal development and following short-term MD.

Considering the effects *circHomer1* depletion had on the morphology of synapses in the No MD condition, we sought to determine how *circHomer1* depletion affected the electrophysiological properties of neurons. We used whole-cell patch clamp recordings in acute slices from P28-33 mice to measure passive membrane and synaptic properties of layer 2/3 neurons infected with either sh-circHomer1 or sh-scramble virus. We did not find any difference in baseline neuronal excitability (Figures S2A–S2F) or the amplitude of miniature excitatory postsynaptic currents (mEPSC; Figures S2G–S2I), but there was a decrease in mEPSC frequency (Figure S2J), consistent with a decrease in protrusion density.[31] The structural and electrophysiological deficits following *circHomer1* depletion were surprising given the normal binocular visual drive observed prior to MD. However, experience-dependent plasticity following MD was delayed as opposed to blocked by *circHomer1* depletion, indicating to us that these deficits were not simply occluding experience-dependent plasticity. We therefore sought to further investigate the mechanism by which *circHomer1* depletion delayed experience-dependent plasticity.

The major mechanism underlying both reduced closed-eye drive and spine shrinkage following MD is a reduction in surface AMPA receptors.[25–27] Therefore, we investigated whether *circHomer1* depletion disrupted surface AMPA receptor trafficking following MD using a biotinylation assay of the AMPA receptor subunit, GluA1 (Figure S3A). As expected, 3-day MD led to a significant reduction of surface GluA1 compared to No MD in sh-scramble mice. There was no reduction of GluA1 levels after 3-day MD in sh-circHomer1 mice (Figure S3A). By 7-day MD, however, there was no significant difference in surface GluA1 expression between sh-scramble and sh-circHomer1 mice. Based on these results, we hypothesized that *circHomer1* was necessary for normal activity-dependent AMPA receptor endocytosis. To examine this further, we treated primary neurons *in vitro* with bicuculline, a $GABA_A$ receptor antagonist, to induce activity-dependent AMPA receptor internalization.[32] 1- or 2-day of treatment with bicuculline induced the upregulation of *circHomer1* in neurons (Figure S3B), and *circHomer1*-depletion impaired bicuculline induced endocytosis of surface AMPA receptors visualized via SEP-GluA1 expression (Figures S3C and S3D). These data demonstrate that *circHomer1* depletion impairs experience- and activity-dependent changes in surface GluA1 expression levels, thus indicating a potential molecular mechanism for the disrupted ocular dominance plasticity and spine shrinkage after 3-day MD.

DISCUSSION

circRNAs are abundantly expressed in mammalian brains, are preferentially derived from genes encoding synaptic proteins,[33,34] and several circRNAs have recently described roles in synaptic plasticity or function.[7–9,21,22] Based on these findings, we performed an unbiased screen to identify candidate experience-dependent plasticity regulated circRNAs using *in vivo* linear- and circular-transcriptome analyses. We identified several promising circRNAs with differential expression in contralateral binocular V1 following 3-day MD in critical period age mice. We focused on *circHomer1*, a well-known circRNA derived from the *Homer1* gene, which encodes important synaptic scaffolding proteins and an activity dependent linear isoform, *Homer1a*, which is a key regulator of glutamatergic synaptic signaling.[35]

circHomer1 and *Homer1a* were differentially regulated by 3-day MD, but in opposing directions, with the expression level of *circHomer1* increasing and that of *Homer1a* decreasing following short-term MD. Following a longer term, 7-day MD, however, expression levels of both *circHomer1* and *Homer1a* were significantly decreased (as measured via RT-qPCR). The developmental expression of *circHomer1* increased rapidly in V1 between P15 and P28, wherein the critical period for ocular dominance plasticity begins, which in combination with its differential expression following 3-day MD, suggested a role for *circHomer1* in critical period plasticity. Indeed, loss of *circHomer1* disrupted ocular dominance plasticity following 3-day MD without affecting baseline visual responses. However, the depletion of *circHomer1* alone also led to less mature dendritic spines and decreased mEPSC frequency. The normal, albeit delayed, expression of ocular dominance plasticity following 7-day MD, however, suggests that the 3-day MD phenotype is not simply a result of occlusion. Indeed, while *circHomer1* depletion impaired 3-day MD induced spine shrinkage and AMPA receptor endocytosis, these effects were not apparent when compared to their respective controls at 7-day MD.

The various proteins derived from the *Homer1* gene play critical roles in regulating synapse development, synaptic strength, and homeostatic synaptic scaling.[36–40] At the postsynaptic density, the activity-dependent short protein isoform of the *Homer1* gene, Homer1a, has dominant-negative effects on the constitutive longer forms of Homer1 (Homer1b/c), and through this interaction regulates the clustering of mGluRs[37–39] and mGluR-dependent NMDA and AMPA receptor currents.[37,41–44] *circHomer1* appears to have a similar dominant negative effect as its linear, activity-dependent counterpart by instead binding directly to dendritic *Homer1b* mRNA which is necessary in the orbitofrontal cortex for normal reversal learning.[21] Despite the fact that Homer1a and *circHomer1* both share activity dependent regulation and antagonize Homer1b expression at the synapse, their regulation by and role in developmental experience-dependent V1 plasticity are clearly distinct. In contrast to

(F) Volume of dendritic spines on apical dendrites (same data as in (D) and (E), values were normalized to 3^3 expansion factor, two-way ANOVA following Tukey multiple comparisons).
(G) Distribution of spine volume in sh-scramble and sh-circHomer1 mice in the 3 conditions (n = 235–334 dendritic spines from 3 mice per group).
Data are presented as mean ± SEM. $^*p < 0.05$; $^{**}p < 0.01$; $^{***}p < 0.001$.

the upregulation of *circHomer1*, *Homer1a* is reduced following 3-day MD (Figure 2B), and depletion of Homer1a does not affect the shift in ODI and reduction of contralateral, closed-eye responses as a result of 3-day MD.[45] Homer1a depletion instead alters the establishment of contralateral bias of V1 responses under basal conditions, which is not affected by *circHomer1* depletion (Figures 3E and 3F). Thus, although both Homer1a and *circHomer1* are regulators of cortical plasticity, they serve different roles in V1 development and experience-dependent plasticity.

It has been shown that the upregulation of activity by bicuculline and 4-Aminopyridine treatment leads to an increase in the expression of the RNA binding protein FUS, which subsequently led to an upregulation of *circHomer1*.[46] However, It remains mechanistically unclear how neuronal activity enhances *circHomer1* expression, as the only demonstrated precursor of *circHomer1* is non-activity dependent *Homer1b* pre-mRNA.[46] Given that activity-dependent *Homer1a* pre-mRNA contains the relevant regions to form *circHomer1*, including a section of intron 5,[46] it is plausible that *circHomer1* could derive from *Homer1a* pre-mRNA, thereby allowing its expression to change in tandem with *Homer1a* mRNA even assuming a fixed ratio of linear/back-splicing, and thus circularization rate. However, during MD and development *in vivo* and bicuculline treatment *in vitro*, we observed timepoints where changes in *circHomer1* expression appear decoupled from or even opposing changes in *Homer1a*. Circular RNA species decay more slowly than their linear counterparts[47] and changes in transcription thus tend to result in larger, longer relative increases in circRNA levels,[48] but this alone seems insufficient to explain this discrepancy. More plausible, perhaps, is that the circularization rate is itself regulated by activity.[46]

Thus, we asked whether a constant circularization rate of *Homer1b* and *Homer1a* pre-mRNA, a variable circularization rate of *Homer1b* pre-mRNA, or a variable circularization rate of both *Homer1b* and *Homer1a* pre-mRNA best fit our observed data (Figure S4A). Our models show that across multiple paradigms, a constant circularization rate of *Homer1a* and *1b* pre-mRNA or a variable circularization rate of *Homer1b* pre-mRNA alone is insufficient to explain the observed expression levels of *circHomer1*. Instead, our data are best fit when adding a variable, activity-dependent circularization rate of both *Homer1b* and *Homer1a* pre-mRNA. In this way, *circHomer1* levels can increase when *Homer1a* mRNA levels do not change or even decrease. Importantly, the model accounts for the bidirectional change in *circHomer1* after 3-day versus 7-day MD. (Figures 2B and S4D). Such regulation could be facilitated by recently described molecular pathways underlying *circHomer1* biogenesis[46] or by changes in other *Homer1* mRNA products not measured in our experiments (for instance, *Homer1b*[21]). Future work is needed to determine if *Homer1a* pre-mRNA can indeed give rise to *circHomer1*, whether the circularization of pre-mRNA occurs at a sufficient frequency to meaningfully decrease linear mRNA availability, and if circular RNA decay rate is static or itself regulated by the activity as is the case for some mRNA species.[7,8,49,50]

An important conclusion of our study is that *circHomer1* has a critical role in the reduction of synaptic drive that accompanies the initiation of MD. Specifically, we found that *circHomer1* knockdown alters the time course of surface GluA1 trafficking during experience-dependent plasticity. However, the exact mechanism of *circHomer1* in synaptic development and plasticity warrants further investigation. Previous studies suggest that *circHomer1* regulates the alternative splicing of mRNA isoforms[9] as well as the synaptic expression of *Homer1b* mRNA in the orbitofrontal cortex via direction competition for HuD binding.[21] Overall expression of several postsynaptic genes was also observed to be downregulated following *circHomer1* knockdown.[22] It remains to be elucidated whether these mechanisms also contribute to the function of *circHomer1* in experience-dependent plasticity.

The mechanism(s) of circRNA function are an area of active investigation. circRNAs are enriched in neurons and are believed to play critical roles in regulating neuronal development and synaptic plasticity.[7–9,33,51] From within the top 100 candidates identified in our MD RNAseq screen, several circRNAs were already reported in the literature to have biological functions in other contexts.[52–54] These include the neuronally enriched circRNA *Cdr1as* (also known as ciRS-7), which has been found to contain a large number of binding sites for miR-7, a regulator of neurodevelopment.[6,55–58] This enrichment for miR-7 binding sites effectively serves as a "miRNA sponge," and *Cdr1as* knockout mice exhibit altered neuronal electrophysiological properties.[6,8] This study identified tens of circRNAs differentially expressed following experience-dependent plasticity and highlights *circHomer1*, a neuron-enriched circRNA derived from the Homer1 gene, as a critical regulator of V1 plasticity during the critical period. Our findings advance the understanding of circRNA regulation during experience-dependent plasticity and shed light on their functional significance in developmental processes.

Limitations of the study

While MD is a well validated method of inducing experience-dependent plasticity,[10–15] it is a very specific form of experience-dependent plasticity; both in that it is largely confined to a developmental critical period and that it is driven by unbalanced input through the two eyes. A less specific manipulation of experience, such as dark rearing/housing and subsequent re-exposure to light, may have uncovered a larger suite of experience-regulated circRNAs, either in place of or in combination with MD.[2,12] As MD results in input (eye) specific changes, we would expect to see the largest ocular dominance shift in binocular V1 neurons receiving input from the deprived eye.[59] Recording from single neurons, either with single-unit electrophysiology or multiphoton calcium imaging, would, therefore, have complimented our mesoscopic imaging of intrinsic hemodynamic signals. In addition, single cell recordings would have resolved other experience-dependent developmental processes, such as binocular matching.[60,61] Furthermore, since no study has reported an association between sex and MD effects,[62] we did not examine the influence of sex on how *circHomer1* regulates experience-dependent plasticity. Finally, despite depleting *circHomer1* only following eye-opening and only in binocular V1, we cannot definitively distinguish whether the resulting impairment in normal ocular dominance plasticity indicates a role for *circHomer1* in gating/permitting such plasticity to occur (ex., through regulating synaptic maturation) or in the expression of excitatory synaptic plasticity itself (ex., through regulating AMPA receptor internalization[15,16]). Future studies investigating the molecular function of *circHomer1* in excitatory

synaptic development and plasticity will allow these two possibilities to be disambiguated.

RESOURCE AVAILABILITY

Lead contact

Requests for further information and resources should be directed to and will be fulfilled by the lead contact, Jacque Pak Kan Ip (jacqueip@cuhk.edu.hk).

Materials availability

All unique/stable reagents generated in this study are available from the lead contact with a completed materials transfer agreement.

Data and code availability

- RNA-seq data have been deposited at GEO (GEO: GSE300377) and are publicly available as of the date of publication. Original western blot images have been deposited at Mendeley and are publicly available as of the date of publication (Mendeley Data: https://doi.org/10.17632/sky4vt8xzh.1). The DOIs is listed in the key resources table.
- Original code has been deposited at Zenodo and is publicly available (Zenodo Data: https://doi.org/10.5281/zenodo.16367030). The DOI is listed in the key resources table.
- Any additional information required to reanalyze the data reported in this article is available from the lead contact upon request.

ACKNOWLEDGMENTS

We thank Jamie Benoit for his contribution to the initial RNA-seq experiment. We thank Taylor Johns, Austin Sullins, and other members of the Sur lab and the Ip lab for their help and support. We thank Hovy Wong for comments on the article. We thank Lorena Rubino for her assistance in analyzing RNA-seq data. We thank Cara Kwong for her technical assistance in neuronal cultures. We thank the MIT BioMicroCenter for running the RNA-seq library preparation and sequencing. We thank scidraw.io for the schematic, licensed under a Creative Commons 4.0 license (https://creativecommons.org/licenses/by/4.0/). This work was supported by NIH grants R01MH085802 (M.S.), R01EY028219 (M.S.), F31EY033649 (K.T.), F32EY032756 (K.J.), The Simons Foundation Autism Research Initiative through the Simons Center for the Social Brain, MIT (M.S.), the National Research Foundation of Korea (RS-2023-00264980; T.K.), the Hong Kong Research Grants Council Early Career Scheme (24117220; J.I), General Research Fund (14117221; J.I.), Area of Excellence Scheme (AoE/M-604/16; J.I., A.F.), Theme-based Research Scheme (T13-605/18-W; J.I., A.F.), Lo Kwee-Seong Biomedical Research Fund (J.I.), Faculty Innovation Awards from the Faculty of Medicine CUHK (FIA2020/A/04; J.I.), and NARSAD Young Investigator Grant from the Brain & Behavior Research Foundation (J.I.).

AUTHOR CONTRIBUTIONS

J.I., N.M., M.N., M.S., and K.J. conceived experiments with input from others. M.N., C.D., and S.Y. performed the cortical dissections and RNA and protein purifications. C.D., M.N, and Y.Z. analyzed RNA-seq data. M.N., Y.C., and C.D. performed qPCR experiments. K.J., K.T., J.Z., and J.I. performed surgeries and viral injection and carried out *in vivo* optical imaging experiments. K.L. analyzed optical imaging data. Y.C., S. Y., and J.Z. performed spine morphology analysis. Y.C., S.Y., T. K., D. Y., and J.I. performed eMAP experiments with inputs from K.C. J.I. performed the surface biotinylation assay and protein analyses. J.S. performed electrophysiological recordings and analyses. Y.C., Y.W., Y.D. performed neuronal culture experiments and relevant analyses. A.F. provided expertise on neuronal culture experiments. N.M. shared the sh-RNA constructs. G.H. performed the modeling of RNA expression. K.J., J.I., and M.S. contributed to the analysis of experiments and interpretation of results. J.I., K.J., and M.S. wrote the article with input from others. All authors edited the article and read and approved the final version.

DECLARATION OF INTERESTS

N.M. is CSO of Circular Genomics Inc, San Diego, CA.

STAR★METHODS

Detailed methods are provided in the online version of this paper and include the following:

- KEY RESOURCES TABLE
- EXPERIMENTAL MODEL AND STUDY PARTICIPANT DETAILS
  - Animals
  - Neuronal cultures, transfection, and pharmacological treatment
- METHOD DETAILS
  - Eyelid suture and monocular deprivation
  - *circHomer1* depletion via shRNA and validation
  - RNA sample preparation
  - RNA sequencing library preparation
  - RNAseq analysis
  - cDNA preparation for qPCR
  - RT-qPCR analysis
  - Optical imaging of intrinsic signals
  - Visual stimulation and optical imaging analysis
  - Epitope-preserving magnified analysis of the proteome (eMAP)
  - Spine morphology and volume analysis
  - Preparation of acute brain slices for electrophysiology
  - Current clamp recordings and analysis
  - mEPSC recordings and analysis
  - Surface protein biotinylation assay
  - Computational modeling
- QUANTIFICATION AND STATISTICAL ANALYSIS

SUPPLEMENTAL INFORMATION

Supplemental information can be found online at https://doi.org/10.1016/j.isci.2025.113421.

Received: April 25, 2025
Revised: June 24, 2025
Accepted: August 19, 2025
Published: August 22, 2025

REFERENCES

1. Yap, E.L., and Greenberg, M.E. (2018). Activity-Regulated Transcription: Bridging the Gap between Neural Activity and Behavior. Neuron *100*, 330–348. https://doi.org/10.1016/j.neuron.2018.10.013.
2. Mellios, N., Sugihara, H., Castro, J., Banerjee, A., Le, C., Kumar, A., Crawford, B., Strathmann, J., Tropea, D., Levine, S.S., et al. (2011). miR-132, an experience-dependent microRNA, is essential for visual cortex plasticity. Nat. Neurosci. *14*, 1240–1242. https://doi.org/10.1038/nn.2909.
3. Chen, W., and Schuman, E. (2016). Circular RNAs in Brain and Other Tissues: A Functional Enigma. Trends Neurosci. *39*, 597–604. https://doi.org/10.1016/j.tins.2016.06.006.
4. Szabo, L., and Salzman, J. (2016). Detecting circular RNAs: bioinformatic and experimental challenges. Nat. Rev. Genet. *17*, 679–692. https://doi.org/10.1038/nrg.2016.114.
5. Chen, L.L. (2020). The expanding regulatory mechanisms and cellular functions of circular RNAs. Nat. Rev. Mol. Cell Biol. *21*, 475–490. https://doi.org/10.1038/s41580-020-0243-y.
6. Kleaveland, B., Shi, C.Y., Stefano, J., and Bartel, D.P. (2018). A Network of Noncoding Regulatory RNAs Acts in the Mammalian Brain. Cell *174*, 350–362.e17. https://doi.org/10.1016/j.cell.2018.05.022.

7. Giusti, S.A., Pino, N.S., Pannunzio, C., Ogando, M.B., Armando, N.G., Garrett, L., Zimprich, A., Becker, L., Gimeno, M.L., Lukin, J., et al. (2024). A brain-enriched circular RNA controls excitatory neurotransmission and restricts sensitivity to aversive stimuli. Sci. Adv. *10*, eadj8769. https://doi.org/10.1126/sciadv.adj8769.

8. Piwecka, M., Glažar, P., Hernandez-Miranda, L.R., Memczak, S., Wolf, S.A., Rybak-Wolf, A., Filipchyk, A., Klironomos, F., Cerda Jara, C.A., Fenske, P., et al. (2017). Loss of a mammalian circular RNA locus causes miRNA deregulation and affects brain function. Science *357*, eaam8526. https://doi.org/10.1126/science.aam8526.

9. Zimmerman, A.J., Hafez, A.K., Amoah, S.K., Rodriguez, B.A., Dell'Orco, M., Lozano, E., Hartley, B.J., Alural, B., Lalonde, J., Chander, P., et al. (2020). A psychiatric disease-related circular RNA controls synaptic gene expression and cognition. Mol. Psychiatry *25*, 2712–2727. https://doi.org/10.1038/s41380-020-0653-4.

10. Sun, Y.J., Espinosa, J.S., Hoseini, M.S., and Stryker, M.P. (2019). Experience-dependent structural plasticity at pre- and postsynaptic sites of layer 2/3 cells in developing visual cortex. Proc. Natl. Acad. Sci. USA *116*, 21812–21820. https://doi.org/10.1073/pnas.1914661116.

11. Hooks, B.M., and Chen, C. (2020). Circuitry Underlying Experience-Dependent Plasticity in the Mouse Visual System. Neuron *106*, 21–36. https://doi.org/10.1016/J.NEURON.2020.01.031.

12. Majdan, M., and Shatz, C.J. (2006). Effects of visual experience on activity-dependent gene regulation in cortex. Nat. Neurosci. *9*, 650–659. https://doi.org/10.1038/nn1674.

13. Hensch, T.K., and Quinlan, E.M. (2018). Critical periods in amblyopia. Vis. Neurosci. *35*, E014. https://doi.org/10.1017/S0952523817000219.

14. Frenkel, M.Y., and Bear, M.F. (2004). How monocular deprivation shifts ocular dominance in visual cortex of young mice. Neuron *44*, 917–923. https://doi.org/10.1016/j.neuron.2004.12.003.

15. Levelt, C.N., and Hübener, M. (2012). Critical-period plasticity in the visual cortex. Annu. Rev. Neurosci. *35*, 309–330. https://doi.org/10.1146/annurev-neuro-061010-113813.

16. Gordon, J.A., and Stryker, M.P. (1996). Experience-Dependent Plasticity of Binocular Responses in the Primary Visual Cortex of the Mouse. J. Neurosci. *16*, 3274–3286. https://doi.org/10.1523/jneurosci.16-10-03274.1996.

17. Tropea, D., Van Wart, A., and Sur, M. (2009). Molecular mechanisms of experience-dependent plasticity in visual cortex. Philos. Trans. R. Soc. Lond. B Biol. Sci. *364*, 341–355. https://doi.org/10.1098/rstb.2008.0269.

18. Espinosa, J.S., and Stryker, M.P. (2012). Development and plasticity of the primary visual cortex. Neuron *75*, 230–249. https://doi.org/10.1016/j.neuron.2012.06.009.

19. Jenks, K.R., Tsimring, K., Ip, J.P.K., Zepeda, J.C., and Sur, M. (2021). Heterosynaptic Plasticity and the Experience-Dependent Refinement of Developing Neuronal Circuits. Front. Neural Circuits *15*, 803401. https://doi.org/10.3389/fncir.2021.803401.

20. Sur, M., Nagakura, I., Chen, N., and Sugihara, H. (2013). Mechanisms of plasticity in the developing and adult visual cortex. Prog. Brain Res. *207*, 243–254. https://doi.org/10.1016/B978-0-444-63327-9.00002-3.

21. Hafez, A.K., Zimmerman, A.J., Papageorgiou, G., Chandrasekaran, J., Amoah, S.K., Lin, R., Lozano, E., Pierotti, C., Dell'Orco, M., Hartley, B.J., et al. (2022). A bidirectional competitive interaction between circHomer1 and Homer1b within the orbitofrontal cortex regulates reversal learning. Cell Rep. *38*, 110282. https://doi.org/10.1016/j.celrep.2021.110282.

22. Zimmerman, A.J., Weick, J.P., Papageorgiou, G., Mellios, N., and Brigman, J.L. (2024). Aberrant encoding of event saliency in the orbitofrontal cortex following loss of the psychiatric-associated circular RNA, circHomer1. Transl. Psychiatry *14*, 480. https://doi.org/10.1038/s41398-024-03188-0.

23. Jakobi, T., Uvarovskii, A., and Dieterich, C. (2019). circtools-a one-stop software solution for circular RNA research. Bioinformatics *35*, 2326–2328. https://doi.org/10.1093/bioinformatics/bty948.

24. Tropea, D., Kreiman, G., Lyckman, A., Mukherjee, S., Yu, H., Horng, S., and Sur, M. (2006). Gene expression changes and molecular pathways mediating activity-dependent plasticity in visual cortex. Nat. Neurosci. *9*, 660–668. https://doi.org/10.1038/nn1689.

25. Nagakura, I., Van Wart, A., Petravicz, J., Tropea, D., and Sur, M. (2014). STAT1 regulates the homeostatic component of visual cortical plasticity via an AMPA receptor-mediated mechanism. J. Neurosci. *34*, 10256–10263. https://doi.org/10.1523/JNEUROSCI.0189-14.2014.

26. Ip, J.P.K., Nagakura, I., Petravicz, J., Li, K., Wiemer, E.A.C., and Sur, M. (2018). Major Vault Protein, a Candidate Gene in 16p11.2 Microdeletion Syndrome, Is Required for the Homeostatic Regulation of Visual Cortical Plasticity. J. Neurosci. *38*, 3890–3900. https://doi.org/10.1523/JNEUROSCI.2034-17.2018.

27. McCurry, C.L., Shepherd, J.D., Tropea, D., Wang, K.H., Bear, M.F., and Sur, M. (2010). Loss of Arc renders the visual cortex impervious to the effects of sensory experience or deprivation. Nat. Neurosci. *13*, 450–457. https://doi.org/10.1038/nn.2508.

28. Kalatsky, V.A., and Stryker, M.P. (2003). New paradigm for optical imaging: temporally encoded maps of intrinsic signal. Neuron *38*, 529–545. https://doi.org/10.1016/s0896-6273(03)00286-1.

29. Peebles, C.L., Yoo, J., Thwin, M.T., Palop, J.J., Noebels, J.L., and Finkbeiner, S. (2010). Arc regulates spine morphology and maintains network stability in vivo. Proc. Natl. Acad. Sci. USA *107*, 18173–18178. https://doi.org/10.1073/pnas.1006546107.

30. Berry, K.P., and Nedivi, E. (2017). Spine Dynamics: Are They All the Same? Neuron *96*, 43–55. https://doi.org/10.1016/j.neuron.2017.08.008.

31. McClelland, A.C., Hruska, M., Coenen, A.J., Henkemeyer, M., and Dalva, M.B. (2010). Trans-synaptic EphB2–ephrin–B3 interaction regulates excitatory synapse density by inhibition of postsynaptic MAPK signaling. Proc. Natl. Acad. Sci. USA *107*, 8830–8835. https://doi.org/10.1073/pnas.0910644107.

32. Shepherd, J.D., Rumbaugh, G., Wu, J., Chowdhury, S., Plath, N., Kuhl, D., Huganir, R.L., and Worley, P.F. (2006). Arc/Arg3.1 mediates homeostatic synaptic scaling of AMPA receptors. Neuron *52*, 475–484. https://doi.org/10.1016/j.neuron.2006.08.034.

33. You, X., Vlatkovic, I., Babic, A., Will, T., Epstein, I., Tushev, G., Akbalik, G., Wang, M., Glock, C., Quedenau, C., et al. (2015). Neural circular RNAs are derived from synaptic genes and regulated by development and plasticity. Nat. Neurosci. *18*, 603–610. https://doi.org/10.1038/nn.3975.

34. Rybak-Wolf, A., Stottmeister, C., Glažar, P., Jens, M., Pino, N., Giusti, S., Hanan, M., Behm, M., Bartok, O., Ashwal-Fluss, R., et al. (2015). Circular RNAs in the Mammalian Brain Are Highly Abundant, Conserved, and Dynamically Expressed. Mol. Cell *58*, 870–885. https://doi.org/10.1016/j.molcel.2015.03.027.

35. Clifton, N.E., Trent, S., Thomas, K.L., and Hall, J. (2019). Regulation and Function of Activity-Dependent Homer in Synaptic Plasticity. Mol. Neuropsychiatry *5*, 147–161. https://doi.org/10.1159/000500267.

36. Diering, G.H., Nirujogi, R.S., Roth, R.H., Worley, P.F., Pandey, A., and Huganir, R.L. (2017). Homer1a drives homeostatic scaling-down of excitatory synapses during sleep. Science *355*, 511–515. https://doi.org/10.1126/science.aai8355.

37. Chokshi, V., Druciak, B., Worley, P.F., and Lee, H.K. (2019). Homer1a is required for establishment of contralateral bias and maintenance of ocular dominance in mouse visual cortex. J. Neurosci. *39*, 3897–3905. https://doi.org/10.1523/JNEUROSCI.3188-18.2019.

38. Hu, J.-H., Park, J.M., Park, S., Xiao, B., Dehoff, M.H., Kim, S., Hayashi, T., Schwarz, M.K., Huganir, R.L., Seeburg, P.H., et al. (2010). Homeostatic Scaling Requires Group I mGluR Activation Mediated by Homer1a. Neuron *68*, 1128–1142. https://doi.org/10.1016/j.neuron.2010.11.008.

39. Martin, S.C., Monroe, S.K., and Diering, G.H. (2019). Homer1a and mGluR1/5 Signaling in Homeostatic Sleep Drive and Output. Yale J. Biol. Med. *92*, 93–101.

40. Tyssowski, K.M., Letai, K.C., Rendall, S.D., Tan, C., Nizhnik, A., Kaeser, P.S., and Gray, J.M. (2019). Firing Rate Homeostasis Can Occur in the Absence of Neuronal Activity-Regulated Transcription. J. Neurosci. *39*, 9885–9899. https://doi.org/10.1523/JNEUROSCI.1108-19.2019.

41. Rozov, A., Zivkovic, A.R., and Schwarz, M.K. (2012). Homer1 gene products orchestrate Ca2+-permeable AMPA receptor distribution and LTP expression. Front. Synaptic Neurosci. *4*, 4. https://doi.org/10.3389/fnsyn.2012.00004.

42. Shin, D., Nam, M., Yoon, Y., and Kim, M. (2010). Membrane-based hybridization capture of intracellular peptide nucleic acid. Anal. Biochem. *399*, 135–137. https://doi.org/10.1016/j.ab.2009.11.031.

43. Yoon, B.J., Smith, G.B., Heynen, A.J., Neve, R.L., and Bear, M.F. (2009). Essential role for a long-term depression mechanism in ocular dominance plasticity. Proc. Natl. Acad. Sci. USA *106*, 9860–9865. https://doi.org/10.1073/pnas.0901305106.

44. Ango, F., Pin, J.P., Tu, J.C., Xiao, B., Worley, P.F., Bockaert, J., and Fagni, L. (2000). Dendritic and axonal targeting of type 5 metabotropic glutamate receptor is regulated by homer1 proteins and neuronal excitation. J. Neurosci. *20*, 8710–8716. https://doi.org/10.1523/JNEUROSCI.20-23-08710.2000.

45. Chokshi, V., Gao, M., Grier, B.D., Owens, A., Wang, H., Worley, P.F., and Lee, H.K. (2019). Input-Specific Metaplasticity in the Visual Cortex Requires Homer1a-Mediated mGluR5 Signaling. Neuron *104*, 736–748.e6. https://doi.org/10.1016/j.neuron.2019.08.017.

46. Mellios, N., Papageorgiou, G., Gorgievski, V., Maxson, G., Hernandez, M., Otero, M., Varangis, M., Dell'Orco, M., Perrone-Bizzozero, N., and Tzavara, E. (2024). Regulation of neuronal circHomer1 biogenesis by PKA/CREB/ERK-mediated pathways and effects of glutamate and dopamine receptor blockade. Preprint at Res. Sq. https://doi.org/10.21203/rs.3.rs-3547375/v1.

47. Enuka, Y., Lauriola, M., Feldman, M.E., Sas-Chen, A., Ulitsky, I., and Yarden, Y. (2016). Circular RNAs are long-lived and display only minimal early alterations in response to a growth factor. Nucleic Acids Res. *44*, 1370–1383. https://doi.org/10.1093/nar/gkv1367.

48. Zhang, Y., Xue, W., Li, X., Zhang, J., Chen, S., Zhang, J.-L., Yang, L., and Chen, L.-L. (2016). The Biogenesis of Nascent Circular RNAs. Cell Rep. *15*, 611–624. https://doi.org/10.1016/j.celrep.2016.03.058.

49. Farris, S., Lewandowski, G., Cox, C.D., and Steward, O. (2014). Selective localization of arc mRNA in dendrites involves activity- and translation-dependent mRNA degradation. J. Neurosci. *34*, 4481–4493. https://doi.org/10.1523/JNEUROSCI.4944-13.2014.

50. Giorgi, C., Yeo, G.W., Stone, M.E., Katz, D.B., Burge, C., Turrigiano, G., and Moore, M.J. (2007). The EJC factor eIF4AIII modulates synaptic strength and neuronal protein expression. Cell *130*, 179–191. https://doi.org/10.1016/j.cell.2007.05.028.

51. Xu, C., Liu, H.J., Qi, L., Tao, C.L., Wang, Y.J., Shen, Z., Tian, C.L., Lau, P.M., and Bi, G.Q. (2020). Structure and plasticity of silent synapses in developing hippocampal neurons visualized by super-resolution imaging. Cell Discov. *6*, 8–11. https://doi.org/10.1038/s41421-019-0139-1.

52. Jeck, W.R., Sorrentino, J.A., Wang, K., Slevin, M.K., Burd, C.E., Liu, J., Marzluff, W.F., and Sharpless, N.E. (2013). Circular RNAs are abundant, conserved, and associated with ALU repeats. RNA *19*, 141–157. https://doi.org/10.1261/rna.035667.112.

53. Liang, D., and Wilusz, J.E. (2014). Short intronic repeat sequences facilitate circular RNA production. Genes Dev. *28*, 2233–2247. https://doi.org/10.1101/gad.251926.114.

54. Zheng, Q., Bao, C., Guo, W., Li, S., Chen, J., Chen, B., Luo, Y., Lyu, D., Li, Y., Shi, G., et al. (2016). Circular RNA profiling reveals an abundant circHIPK3 that regulates cell growth by sponging multiple miRNAs. Nat. Commun. *7*, 11215. https://doi.org/10.1038/ncomms11215.

55. Choudhury, N.R., de Lima Alves, F., de Andrés-Aguayo, L., Graf, T., Cáceres, J.F., Rappsilber, J., and Michlewski, G. (2013). Tissue-specific control of brain-enriched miR-7 biogenesis. Genes Dev. *27*, 24–38. https://doi.org/10.1101/gad.199190.112.

56. Hansen, T.B., Jensen, T.I., Clausen, B.H., Bramsen, J.B., Finsen, B., Damgaard, C.K., and Kjems, J. (2013). Natural RNA circles function as efficient microRNA sponges. Nature *495*, 384–388. https://doi.org/10.1038/nature11993.

57. Memczak, S., Jens, M., Elefsinioti, A., Torti, F., Krueger, J., Rybak, A., Maier, L., Mackowiak, S.D., Gregersen, L.H., Munschauer, M., et al. (2013). Circular RNAs are a large class of animal RNAs with regulatory potency. Nature *495*, 333–338. https://doi.org/10.1038/nature11928.

58. Rajman, M., and Schratt, G. (2017). MicroRNAs in neural development: from master regulators to fine-tuners. Development *144*, 2310–2322. https://doi.org/10.1242/dev.144337.

59. Mrsic-Flogel, T.D., Hofer, S.B., Ohki, K., Reid, R.C., Bonhoeffer, T., and Hübener, M. (2007). Homeostatic regulation of eye-specific responses in visual cortex during ocular dominance plasticity. Neuron *54*, 961–972. https://doi.org/10.1016/j.neuron.2007.05.028.

60. Wang, B.S., Sarnaik, R., and Cang, J. (2010). Critical period plasticity matches binocular orientation preference in the visual cortex. Neuron *65*, 246–256. https://doi.org/10.1016/j.neuron.2010.01.002.

61. Tan, L., Tring, E., Ringach, D.L., Zipursky, S.L., and Trachtenberg, J.T. (2020). Vision Changes the Cellular Composition of Binocular Circuitry during the Critical Period. Neuron *108*, 735–747.e6. https://doi.org/10.1016/j.neuron.2020.09.022.

62. Steinwurzel, C., Pennella, G., and Binda, P. (2025). Short-term monocular deprivation in adult humans: a meta-analysis and new perspectives. Preprint at bioRxiv. https://doi.org/10.1101/2025.02.20.639298.

63. Kim, D., Paggi, J.M., Park, C., Bennett, C., and Salzberg, S.L. (2019). Graph-based genome alignment and genotyping with HISAT2 and HISAT-genotype. Nat. Biotechnol. *37*, 907–915. https://doi.org/10.1038/s41587-019-0201-4.

64. Liao, Y., Smyth, G.K., and Shi, W. (2014). featureCounts: an efficient general purpose program for assigning sequence reads to genomic features. Bioinformatics *30*, 923–930. https://doi.org/10.1093/bioinformatics/btt656.

65. Love, M.I., Huber, W., and Anders, S. (2014). Moderated estimation of fold change and dispersion for RNA-seq data with DESeq2. Genome Biol. *15*, 550. https://doi.org/10.1186/s13059-014-0550-8.

66. Ritchie, M.E., Phipson, B., Wu, D., Hu, Y., Law, C.W., Shi, W., and Smyth, G.K. (2015). limma powers differential expression analyses for RNA-sequencing and microarray studies. Nucleic Acids Res. *43*, e47. https://doi.org/10.1093/nar/gkv007.

67. Yu, G., Wang, L.G., Han, Y., and He, Q.Y. (2012). clusterProfiler: an R package for comparing biological themes among gene clusters. OMICS *16*, 284–287. https://doi.org/10.1089/omi.2011.0118.

68. Wang, Y., Fu, W.Y., Cheung, K., Hung, K.W., Chen, C., Geng, H., Yung, W.H., Qu, J.Y., Fu, A.K.Y., and Ip, N.Y. (2021). Astrocyte-secreted IL-33 mediates homeostatic synaptic plasticity in the adult hippocampus. Proc. Natl. Acad. Sci. USA *118*, e2020810118. https://doi.org/10.1073/pnas.2020810118.

69. Ku, T., Swaney, J., Park, J.Y., Albanese, A., Murray, E., Cho, J.H., Park, Y.G., Mangena, V., Chen, J., and Chung, K. (2016). Multiplexed and scalable super-resolution imaging of three-dimensional protein localization in size-adjustable tissues. Nat. Biotechnol. *34*, 973–981. https://doi.org/10.1038/nbt.3641.

70. Park, J., Khan, S., Yun, D.H., Ku, T., Villa, K.L., Lee, J.E., Zhang, Q., Park, J., Feng, G., Nedivi, E., and Chung, K. (2021). Epitope-preserving magnified analysis of proteome (eMAP). Sci. Adv. *7*, eabf6589. https://doi.org/10.1126/sciadv.abf6589.

71. Chen, T., He, H.L., and Church, G.M. (1999). Modeling gene expression with differential equations. Pac. Symp. Biocomput. *4*, 29–40.

72. Bachmayr-Heyda, A., Reiner, A.T., Auer, K., Sukhbaatar, N., Aust, S., Bachleitner-Hofmann, T., Mesteri, I., Grunt, T.W., Zeillinger, R., and Pils, D. (2015). Correlation of circular RNA abundance with proliferation–exemplified with colorectal and ovarian cancer, idiopathic lung fibrosis, and normal human tissues. Sci. Rep. *5*, 8057. https://doi.org/10.1038/srep08057.

STAR★METHODS

KEY RESOURCES TABLE

REAGENT or RESOURCE	SOURCE	IDENTIFIER
Antibodies		
Rabbit polyclonal anti-Homer1	Synaptic Systems	Cat#160003; RRID: AB_887730
Mouse monoclonal anti-α-Tubulin	Santa Cruz	Cat#sc32293; RRID: AB_628412
Chicken polyclonal anti-GFP	Invitrogen	Cat#A10262; RRID: AB_2534023
Rabbit monoclonal anti-GluA1	Sigma-Aldrich	Cat#04-855; RRID: AB_1977216
Rabbit polyclonal anti-pan Cadherin	Abcam	Cat#ab6529; RRID: AB_305545
Bacterial and virus strains		
AAV2/9-hSyn-DIO-EGFP	BrainVTA	Cat#PT-1103
AAV2/9-CaMKIIa-Cre	BrainVTA	Cat#PT-0220
AAV9-U6-scramble shRNA-CMV-DsRed	Vigene	N/A
AAV9-U6-*circHomer1* shRNA-CMV-DsRed	Vigene	N/A
pLV-mU6-scrambled-shRNA::SYN-tdTomato	System Biosciences	N/A
pLV-mU6-*circHomer1*a shRNA::SYN-tdTomato	System Biosciences	N/A
Chemicals, peptides, and recombinant proteins		
Bicuculline	Sigma-Aldrich	Cat#14340
TRIzol	Ambion	Cat#15596-026
Lysing Matrix D	MPBio	Cat#116913050
Critical commercial assays		
Zymo RNA Clean & Concentrator-5	Zymo Research	Cat#R1016
SuperScript IV VILO (SSIV VILO) Master Mix	Invitrogen	Cat#11766050
PowerUp SYBR Green Master Mix	Applied Biosystems	Cat#A25742
NucleoSpin RNA Mini kit	Macherey-Nagel	Cat#740955
Deposited data		
RNA sequencing data	This paper	GEO Datasets: GSE300377
Original code	This paper	Zenodo Data: https://doi.org/10.5281/zenodo.16367030
Original western blot images	This paper	Mendeley Data: https://doi.org/10.17632/sky4vt8xzh.1
Experimental models: Organisms/strains		
Mouse: C57BL/6J	Jackson Laboratory or CUHK's Laboratory Animal Services Center	JAX000664
Rat: Sprague-Dawley	CUHK's Laboratory Animal Services Center	Rat Genome Database ID: 737903
Recombinant DNA		
pLV-mU6-scrambled-shRNA::SYN-tdTomato	Biosettia	N/A
pLV-mU6-*circHomer1*-shRNA::SYN-tdTomato	Biosettia	N/A
pCI-SEP-GluR1	Addgene	Addgene Plasmid #24000
Software and algorithms		
Graphpad Prism	GraphPad Prism (https://www.graphpad.com/)	Version 10
ImageJ	ImageJ (https://imagej.net/ij/)	N/A
Imaris	Imaris (https://imaris.oxinst.com/)	Version 10
Mini Analysis	Synaptosoft	Version 6
lmfit	lmfit (https://lmfit.github.io/lmfit-py/)	N/A
HISAT2	Kim et al.[63]	PMID: 31375807
featureCounts	Liao et al.[64]	PMID: 24227677
DESeq2	Love et al.[65]	PMID: 25516281

(*Continued on next page*)

Continued

REAGENT or RESOURCE	SOURCE	IDENTIFIER
circtools	Jakobi et al.[23]	PMID: 30462173
Limma	Ritchie et al.[66]	PMID: 25605792
clusterProfiler	Yu et al.[67]	PMID: 22455463

EXPERIMENTAL MODEL AND STUDY PARTICIPANT DETAILS

Animals

Experiments were carried out in mice under protocols conforming to NIH guidelines and approved by MIT's Animal Care and Use Committee (protocol number 2308000562) or by CUHK's Animal Experimentation Ethics Committee (approval number 21/104/NSF). Wildtype C57BL/6J mice (JAX000664) were sourced from Jackson Laboratory or CUHK's Laboratory Animal Services Center. Mice were group-housed whenever possible with up to 5 same-sex mice per cage. The cages were in a standard animal facility room with a 12-h/12-h light/dark cycle. Food and water were available *ad libitum*. Both male and female mice were used for experiments. P15 and P25 mice were used for virus injection and monocular deprivation experiments, respectively.

Neuronal cultures, transfection, and pharmacological treatment

Cultured primary rat hippocampal and cortical cells were prepared from Sprague–Dawley rat embryos sacrificed on embryonic day 18.[68] The hippocampus and cortices were dissected, and the cells were dissociated with trypsin. Hippocampal cells were cultured on 18-mm coverslips coated with 1 mg/mL poly-D-lysine at 1×10^5 cells per coverslip in Neurobasal Plus medium supplemented with 2% B27 Plus and 0.5 mM L-glutamate. Cortical cells were cultured on 60-mm cultural dishes coated with 100 μg/mL poly-L-lysine at 3×10^6 per dish in Neurobasal medium supplemented with 2% B27 and 10 mM glucose. All cells were maintained at 37 °C in a humidified atmosphere with 5% CO_2. The cortical neurons were treated with bicuculine (20 μM) at DIV 13. Total RNA of cortical neurons was extracted at 0, 2, 6, 24, or 48 h later using NucleoSpin RNA Mini kit (Macherey-Nagel, 740955) according to the manufacturer's protocol. The hippocampal neurons at DIV 11 were transfected with a *circHomer1* (GCCATTTCCACATAGGGAGCA) or scrambled control shRNA construct and SEP-GluA1 using calcium phosphate precipitation.[68] The transfected neurons were then treated with bicuculine (20 μM, 48 h) for subsequent analysis. At DIV 19 the hippocampal neurons were fixed with 4% PFA, and blocking was performed for 1 h at room temperature with 1% BSA in PBS. Antibody against GFP (A10262, Invitrogen) was diluted in 1% BSA in PBS and incubated with cells at 4°C overnight. After washing with PBS, the cells were incubated with secondary antibody for 1 h at room temperature. The cells were then washed with PBS and mounting was performed. Imaging was performed under Leica SP8 confocal microscope using a 63× oil immersion lens with 1.4 numerical aperture.

METHOD DETAILS

Eyelid suture and monocular deprivation

For monocular deprivation experiments, mice were anesthetized using 2–3% isoflurane. The top and bottom eyelid of the right eye was trimmed, and sterile nylon sutures (7-0) were used to suture the eyelid, which were further sealed with Vetbond (3M). The suture was inspected for the next 3–7 days post-closure to ensure that the eye did not reopen. Mice that exhibited incomplete eyelid closure were removed from the experiment.

circHomer1 depletion via shRNA and validation

For *circHomer1* depletion experiments, the following viruses were used: lentivirus expressing pLV-mU6-scrambled-shRNA::SYN-tdTomato or pLV-mU6-*circHomer1*a-shRNA::SYN-tdTomato (1.2×10^9 IFU/mL, System Biosciences), or AAV9 expressing pAV-U6-sh-scramble-CMV-DsRed or pAV-U6-sh-circHomer1-CMV-DsRed (2×10^{13} vg/mL, Vigene). For the *in vivo* shRNA experiments, binocular V1 in the left hemisphere of P15 pups was targeted. Briefly, sh-scrambled or sh-circHomer1 viruses were loaded into a pulled-glass micropipette with a beveled tip, lowered into L2/3, and virus was infused at a rate of 100 nL/min. The following coordinates were used (in mm from lambda at P15): AP: 0.5 to 1.0; ML: −2.8, DV:-0.2 to −0.25. A minimum of 10 days was allowed for viral transduction and sufficient expression of the constructs in all experiments. To estimate the efficiency and specificity of sh-circHomer1 after virus injection, the mouse brain was examined using a dual fluorescent protein flashlight (Nightsea) after mouse sacrifice and dissection. The tissue expressing RFP was dissected for RNA purification for RT-qPCR (see below), and protein isolation for Western blot. For protein isolation, the RFP-expressing tissue were homogenized in RIPA buffer (1% NP40, 0.1% SDS and 0.5% sodium deoxycholate in PBS). The homogenate was centrifuged at 14,000 × g for 15 min and the supernatant was collected. Protein concentration was measured by BCA protein assay, and 20 μg total protein lysate was boiled for 5 min with 6× loading buffer. Standard Western blot was performed. Data are displayed normalized to the mean intensity of bands from sh-scramble group. Antibodies used include Homer1 (160003; Synaptic Systems) and α-Tubulin (sc32293; Santa Cruz).

RNA sample preparation

RNA was extracted from fresh tissue. Tissue for RNA extraction was isolated from V1 contralateral and ipsilateral to the sutured eye after 3-day MD (at P28), 7-day MD (at P32) or from mice that had not undergone MD (various ages based on experiment). Briefly, mice were anesthetized with isoflurane and transcardially perfused with ice-cold phosphate buffered saline (PBS) for at least 5 min. A sterile scalpel blade and forceps were used to surgically micro-dissect the appropriate tissue section. The dissected tissue was immediately placed into a 2-mL lysing tube containing 1.4 mm spherical ceramic beads (MPBio, Lysing Matrix D, Cat. No. 116913050) and pre-filled with 1 mL of ice-cold TRIzol (Ambion, Cat. No. 15596-026) and then immediately homogenized with a bead-based homogenizer (FastPrep-24 5G, MPBio) using the preset settings for mouse brain tissue (8.0 m/s, 30 s). Once foaming has subsided at room temperature, the homogenate was transferred into 2 mL Phase Lock Tube (Heavy; 5Prime Bio, Cat. No. 2302830) pre-filled with 200 μL chloroform and briefly vortexed. Samples were centrifuged at 12,000 × g for 10 min at 2°C–4°C. The colorless upper aqueous layer was then transferred into a new 2.0 mL LoBind tube that was pre-filled with 1.5 volumes of 100% EtOH (~600 μL), then mixed thoroughly by pipetting up and down several times, and then briefly centrifuged. The sample was furthered purified using Zymo RNA Clean & Concentrator-5 (Zymo Research, R1016) according the manufacturer's recommended protocol and always performed with the optional in-column DNase I treatment. RNA was eluted twice with ≥6 μL 1× TE buffer (pH 7.5). The approximate concentration and relative purity of RNA was determined using a NanoDrop 2000 spectrophotometer (Thermo Scientific). The purified RNA was either immediately used for downstream applications (i.e., reverse transcription) or stored at −80°C.

RNA sequencing library preparation

For samples to be sequenced, RNA quality was assessed using AATI Fragment Analyzer. Samples with RNA Quality Number of >8.0 were further processed. Indexed cDNA libraries were generated using the SMARTer Stranded Total RNA-Seq Kit v2 and multiplexed sequencing was performed on Illumina HiSeq 2000 or Novaseq 6000.

RNAseq analysis

Read alignment was performed using HISAT2.[63] The mRNA counts were obtained using featureCounts.[64] Differential expression analysis was performed using DESeq2.[65] The circRNA counts were obtained using circtools.[23] Differential expression analysis was performed using the Bioconductor package Limma.[66] Gene Ontology enrichment analysis was performed using the Bioconductor package clusterProfiler.[67] Differential expression analysis of 3-day MD RNAseq data was performed comparing the contralateral side and ipsilateral side within animal. For 7-day MD RNAseq, differential expression analysis was performed comparing control, no MD animals and MD animals (contralateral side).

cDNA preparation for qPCR

Total RNA was reversed transcribed using SuperScript IV VILO with ezDNase treatment (Thermo Fisher, Cat. No. 11766050) according to manufacturer's recommended protocol with the following modifications: the maximum input of total RNA was lowered to 2 μg per 20 μL reaction, ezDNase digestion was extended to 5 min, and reverse transcription temperature was increased to 55°C. After the RT reaction, cDNA was diluted with 1× TE buffer (pH 8.0).

RT-qPCR analysis

Applied Biosystems QuantStudio 3 Fast thermocycler was used for all qPCR amplification and detection in this study. PowerUp SYBR Green Master Mix (Applied Biosystems, Cat. No. A25742) was used according to the manufacturer's recommended protocol. Primers used are listed in Table S3. RT-qPCR data were analyzed by first normalizing the quantity of our target linear or circular RNA (measured by Ct) to *Gapdh* within the same sample for both the experimental and control group (target Ct – *Gapdh* Ct = ΔCt). Then, *Gapdh* normalized ΔCt values were compared between experimental (contra V1 for Figure 2B; V1 of different postnatal ages for Figure 2C; sh-circHomer1 injected V1 for Figure 3A; cells of different treatment time for Figure S3B) and control groups (ipsi V1 from the same mouse for Figure 2B; mean of P0 timepoint for Figure 2C; mean of sh-scramble injected V1 for Figure 3A; mean of 0 h timepoint for Figure S3B) [Experimental ΔCt – control ΔCt = ΔΔCt]. Data are displayed as relative expression ($2^{(-\Delta\Delta Ct)}$) of the experimental group to the control group.

Optical imaging of intrinsic signals

At postnatal day P15, sh-scramble or sh-circHomer lenti-viral vectors were injected into left binocular V1 as described above, and at P22 a 3 mm craniotomy was performed over the same area, where a 5 mm diameter glass window stacked on top of a 3 mm diameter glass window was fitted over the craniotomy with dental cement, together with a metal headplate. Baseline optical imaging was performed at P25, prior to MD. MD lasted either 3 days or 7 days, after which sutures were removed and the closed eye was reopened under isoflurane anesthesia before optical imaging experiments to assess the effects of 3-day or 7-day MD on V1 responses.[26] Mice were lightly anesthetized with isoflurane (0.5–1%), the window was cleaned with 70% ethanol and a cotton tipped applicator, and the headplate was attached to the imaging rig to minimize head movements. Green light (560 nm) was used to focus 400 μm below the cortical surface. Red light (630 nm) was used for functional imaging, and the change in reflectance was captured by an electron multiplying CCD camera (Cascade 512B; Roper Scientific) during the presentation of visual stimuli.

Visual stimulation and optical imaging analysis

The visual stimulus was a horizontal bar 30° wide, made of flickering checkerboard over a black background, drifting continuously through the peripheral–central dimension of the visual field. After moving to the last position, the bar would jump back to the initial position and start another cycle of movement; therefore, the chosen region of visual space (72 ° × 72 °) was stimulated in a periodic manner (12 s/cycle, 20 repetitions). Images were continuously captured at the rate of 30 frames/s during each stimulus session of 4 min, with a separate stimulus session for each of the 4 cardinal directions. A temporal component at the stimulus frequency ($12s^{-1}$) was calculated pixel by pixel from the whole set of images using custom python scripts (https://github.com/Palpatineli/oi_analyzer). The amplitude of the FFT component was used to measure the strength of visually driven response for each eye, and the ODI was derived from the response (R) of each eye at each pixel as ODI = $(R_{contralateral} - R_{ipsilateral})/(R_{contralateral} + R_{ipsilateral})$. The binocular zone was defined as the cortical region that was driven by both eyes. The response amplitude for each eye was defined as fractional changes in reflectance over baseline reflectance ($\Delta R/R \times 10^{-3}$), and the top 50% pixels were analyzed to avoid background contamination.

Epitope-preserving magnified analysis of the proteome (eMAP)

Mice were injected at P15 as described above with AAV2/9-hSyn-DIO-EGFP (1×10^{13} vg/mL), AAV2/9-CaMKIIa-Cre (5×10^{8} vg/mL), and AAV9 expressing either pAV-U6-sh-scramble-CMV-DsRed or pAV-U6-sh-circHomer1-CMV-DsRed (1×10^{13} vg/mL). Animals were allowed to express virus for a minimum of 10 days before MD. After MD, mice were transcardially perfused under deep anesthesia with ice-cold PBS followed by ice-cold 4% PFA (in PBS), and then brains were post-fixed in 4% PFA at 4°C overnight. eMAP processing was performed following established protocols.[69,70] Tissue embedding was performed using eMAP solution (30% acrylamide, 10% sodium acrylate, 0.1% bisacrylamide, 0.03% VA-044 in PBS) under vacuum, following hydration using hydration solution (0.02% sodium azide in PBS) and sectioning into 60 μm thick using a Leica VT1000S vibratome. Tissue clearing was performed by incubation in clearing solution (6% SDS, 0.1 M phosphate buffer, 50 mM sodium sulfite, 0.02% sodium azide in DI water, pH 7.4) at 37°C for 4 h. If applicable, after washing with PBST (0.1% Triton X-100, 0.02% sodium azide in PBS), samples were stained with primary antibody against GFP (A10262, Invitrogen) diluted in PBST at 37°C for 48 h. After washing with PBST, samples were stained with secondary antibodies diluted in PBST for 48 h. Expansion was performed using 0.01× PBS before imaging. Approximately 3× total linear expansion was achieved consistently. Pyramidal neurons in V1 which were double-positive for RFP and GFP were identified and imaged using a Leica SP8 confocal microscope with 20 × 0.75 NA or 63 × 1.2 NA water immersion lens.

Spine morphology and volume analysis

Dendrites and dendritic spines for analysis were selected and analyzed by an experimenter blinded to experiment condition. To analyze dendritic spine morphology, the length (L), head width (H), and neck width (N) were measured by ImageJ. Dendritic spines were classified into 4 types according to established criteria.[29] The average length of spine head in the No MD sh-scramble group ($\overline{H}$) was calculated. Protrusions with $H > N$ and $H > \overline{H}$ were defined as mushroom spines; protrusions with $H > N$ and $H < \overline{H}$ were defined as thin spines; protrusions with $H \leq N$ and $L < \overline{H}$ were defined as stubby spines, and protrusions with $H \leq N$ and $L > 1.5^{*} \overline{H}$ were defined as filopodia. For dendritic spine volume analysis, 3D reconstruction and quantification of dendritic spines volume was performed using the "Filament" function in Imaris software. The raw data was then divided by 3^3 (=27) to convert to values that closely approximates the unexpanded volume.

Preparation of acute brain slices for electrophysiology

Mice injected with either sh-scramble or sh-circHomer1 lentivirus (as described above) were anesthetized with 2–3% isoflurane and decapitated. Brains were rapidly removed and placed into ice-cold low-Ca2+, low-Na+ sucrose cutting solution consisting of (in mM): 234 sucrose, 11 glucose, 24 $NaHCO_3$, 2.5 KCl, 1.25 NaH_2PO_4, 10 $MgSO_4$, and 0.5 $CaCl_2$. Cutting solution was oxygenated with a mixture of 95% O_2 and 5% CO_2. 300 μM slices were cut in a coronal orientation using a vibratome (Leica Biosystems, Buffalo Grove, IL) and placed into a recovery chamber filled with oxygenated ACSF consisting of (in mM): 126 NaCl, 2.5 KCl, 1.25 NaH_2PO_4, 1 $MgSO_4$, 2 $CaCl_2$, 10 glucose, and 26 $NaHCO_3$. Slices were allowed to recover at 34°C for 1 h before being kept at room temperature (25°C) for the remainder of the experiment.

Current clamp recordings and analysis

TdTomato-positive neurons were identified in Layer 2/3 of the V1 binocular region. Recordings were made at 34°C in ACSF containing 10 μM CPP, 20 μM DNQX, and 10 μM SR95531 to isolate passive membrane properties. Signals were collected at 10 kHz using a Multiclamp 700B amplifier and digitized using a Digidata 1440A (Molecular Devices, San Jose, CA). Whole-cell patch clamp recordings were made using borosilicate glass electrode with an open-tip resistance of 2–5 MΩ filled with an intracellular solution consisting of (in mM): 130 potassium gluconate, 10 HEPES, 5 KCl, 5 EGTA, 2 NaCl, 1 $MgCl_2$, 10 TEA-Cl, 10 phosphocreatine, 2 Mg-ATP, and 0.3 Na-GTP (pH adjusted to 7.28, osmolarity adjusted to 290 mOsm). Current steps of 250 ms duration were applied, from −100 pA increasing to 650 pA at 25 pA increments. The holding current was returned to 0 pA for 750 ms between each current injection step. Ra (access resistance) and Rm (membrane resistance) were also measured in response to a 5 mV depolarizing step, and membrane capacitance was calculated as $C = \frac{\tau}{Rm}$, where τ is the decay of the capacitive transient in response to the 5 mV step. Access resistance was monitored throughout the recording and recordings with >20% change in access resistance or with access resistance >30 MΩ were excluded.

mEPSC recordings and analysis

Slices were prepared as above. Recordings of tdTomato positive neurons were made at 34°C in ACSF containing 10 μM CPP, 10 μM SR95531, and 1 μM tetrodotoxin to isolate miniature AMPA receptor-mediated currents. Signals were collected at 10 kHz and filtered at 2 kHz using a Multiclamp 700B amplifier and digitized using a Digidata 1440A (Molecular Devices, San Jose, CA). Whole-cell patch clamp recordings were established using borosilicate glass electrode with an open-tip resistance of 2–5 MΩ filled with an intracellular solution consisting of (in mM): 100 potassium gluconate, 10 HEPES, 20 KCl, 0.5 EGTA, 10 NaCl, 8 phosphocreatine, 2 Mg-ATP, and 0.3 Na-GTP (pH adjusted to 7.23, osmolarity adjusted to 290 mOsm). Neurons were voltage-clamped at −70 mV and stable gap free recordings were made for at least 2 min. Access resistance was monitored throughout the recording and recordings with >20% change in access resistance or with access resistance >30 MΩ were excluded. mEPSC events were detected using the MiniAnalysis software (Synaptosoft, Fort Lee, NJ).

Surface protein biotinylation assay

For the measurement of surface proteins, we first prepared 300 μm acute coronal slices containing V1 in ice-cold ACSF and then washed slices 3 times in ice-cold ACSF in 6-well plate on shaker. The sections were incubated in 100 μM S-NHS-SS-biotin for 45 min (~1 mL per well). The superficial layers of V1 were dissected into a new 1.5 mL tube filled with ice-cold ACSF and homogenize in RIPA buffer. The homogenate was centrifuged at 14,000 × g for 5 min and the supernatant was transferred into a new 1.5 mL tube. ~20% volume was transferred into a new 1.5 mL tube and stored at −80°C to be used later as a total protein control. ACSF was added to the remaining supernatant for a final volume of 1 mL per sample. 40 μL of streptavidin beads were added and incubated on a shaker overnight at 4°C. Samples were then centrifuged at 3,500 × g for 1 min. The supernatant was discarded and then the beads were washed 3× in 1:1 v/v ice-cold solution of ACSF and RIPA buffer. Then, 40 μL of 2× loading buffer was added, mixed briefly, and boiled for 5 min. Standard Western blot was performed. Antibodies used include GluA1 (04–855, clone C3T; Millipore), and pan-Cadherin (ab6529; Abcam).

Computational modeling

As it is unclear what stages in the biogenesis of *circHomer1* confer its activity-dependence, we compared three nested dynamical system models[71] of *circHomer1* expression with the same basic architecture to assess which best fit our data. We modeled three time-varying outputs: (1) *Homer1b* mRNA levels (H1b), (2) *Homer1a* mRNA levels (H1a), and (3) *circHomer1* RNA levels (CH). Dynamical changes in gene expression were described by the following differential equations:

$$\Delta H1a = (H1aTR - decL \cdot H1a - H1aC \cdot CR \cdot H1a)dt$$

$$\Delta H1b = (H1bTR - decL \cdot H1b - CR \cdot H1b)dt$$

$$\Delta CH = (CR \cdot H1b + H1aC \cdot CR \cdot H1a - decCH \cdot CH)dt$$

with H1a/bTR denoting transcription rates of pre-mRNA, decL denoting linear mRNA decay rate, decCH denoting circular RNA decay rate, CR denoting circularization rate, and H1aC denoting a logical operator of whether *Homer1a* can be circularized (1 if true, 0 if false). Parameters were fit separately for each model/experiment combination, but the fit parameter values for a particular model were largely consistent across experiments.

We hypothesized[21,46] that the activity-dependence of *circHomer1* expression was most likely to arise from circularization of an activity-dependent pre-mRNA (*Homer1a*) and/or activity dependent circularization of a constitutively expressed pre-mRNA (*Homer1b*). The three models tested were as follows. (1) The constant circularization model fit a constant circularization rate of pre-*Homer1a* and pre-*Homer1b*, with the only time varying parameter being the transcription rate of *Homer1a* which was fit to measured data. (2) The variable circularization model allowed the circularization rate to vary over time, however only pre-*Homer1b* could be circularized. (3) The third, full model also included time varying circularization but both pre-*Homer1b* and pre-*Homer1a* could be circularized. *Homer1a* and *circHomer1* levels were explicitly fit to minimize squared error from observed datapoints for each experiment. *Homer1b* levels were treated as a 'hidden' variable; as they were not measured experimentally and were not a part of model testing.

Models were initialized 10 days before the first timepoint to allow RNA levels to stabilize before permitting any changes in transcription or circularization. Because of the varied measurements and methods across experiments, data in each model were normalized to the first timepoint, T = 0. In models where circularization of pre-*Homer1a* was permitted, the same circularization rate was applied to both pre- *Homer1a* and *Homer1b* pools. Fit circularization rates were 1–2 orders of magnitude smaller than the linear splicing rates,[72] and varied with activity by at most a factor of 4. In each of the models, the decay rate of *circHomer1* was constrained to be slower than that of linear *Homer1* mRNA by a factor of ≥2.[47] All models were run with 15 min timesteps. *Homer1b* transcription rate, linear decay rate, and circular decay rate were fit as constant parameters in each model. *Homer1a* transcription rate was fit as a variable parameter in each model. Circularization rate was fit as a constant parameter in the constant circularization model, and a variable parameter in the variable circularization and full model. Fitting was performed and AIC scores for each model were computed using the python package lmfit.

QUANTIFICATION AND STATISTICAL ANALYSIS

Data are presented as mean ± standard error of the mean (SEM) in quantitative analysis unless other specified. When two independent experimental groups were analyzed, Student's t test was performed, while paired t-test was performed when two paired experimental data were analyzed. One sample t-test was performed for analyzing the relative expression of linear and circular RNAs in contra/ipsi V1 following MD. When more than two independent experimental groups were analyzed, one-way ANOVA followed by Tukey post hoc test was performed. For those experiments exploring the effect of *circHomer1* during MD by *circHomer1* depletion, two-way ANOVA followed by Tukey post hoc test was performed. For optical imaging, mixed-effects model following Holm-Sidak multiple comparisons test was performed. For mEPSC quantification, two-sample Kolmogorov-Smirnoff test was performed. Statistical significance was defined as $p < 0.05$. Statistical details for each experiment can be found in the associated figure legends and Table S4.

iScience, Volume *28*

Supplemental information

The noncoding circular RNA *circHomer1* regulates synaptic development and experience-dependent plasticity in the mouse visual cortex

Kyle R. Jenks, Ying Cai, Marvin Eduarte Nayan, Katya Tsimring, Keji Li, José C. Zepeda, Gregg R. Heller, Chloe Delepine, Jennifer Shih, Shiyang Yuan, Yao Zhu, Ye Wang, Yangyang Duan, Amy K.Y. Fu, Taeyun Ku, Dae Hee Yun, Kwanghun Chung, Nikolaos Mellios, Mriganka Sur, and Jacque Pak Kan Ip

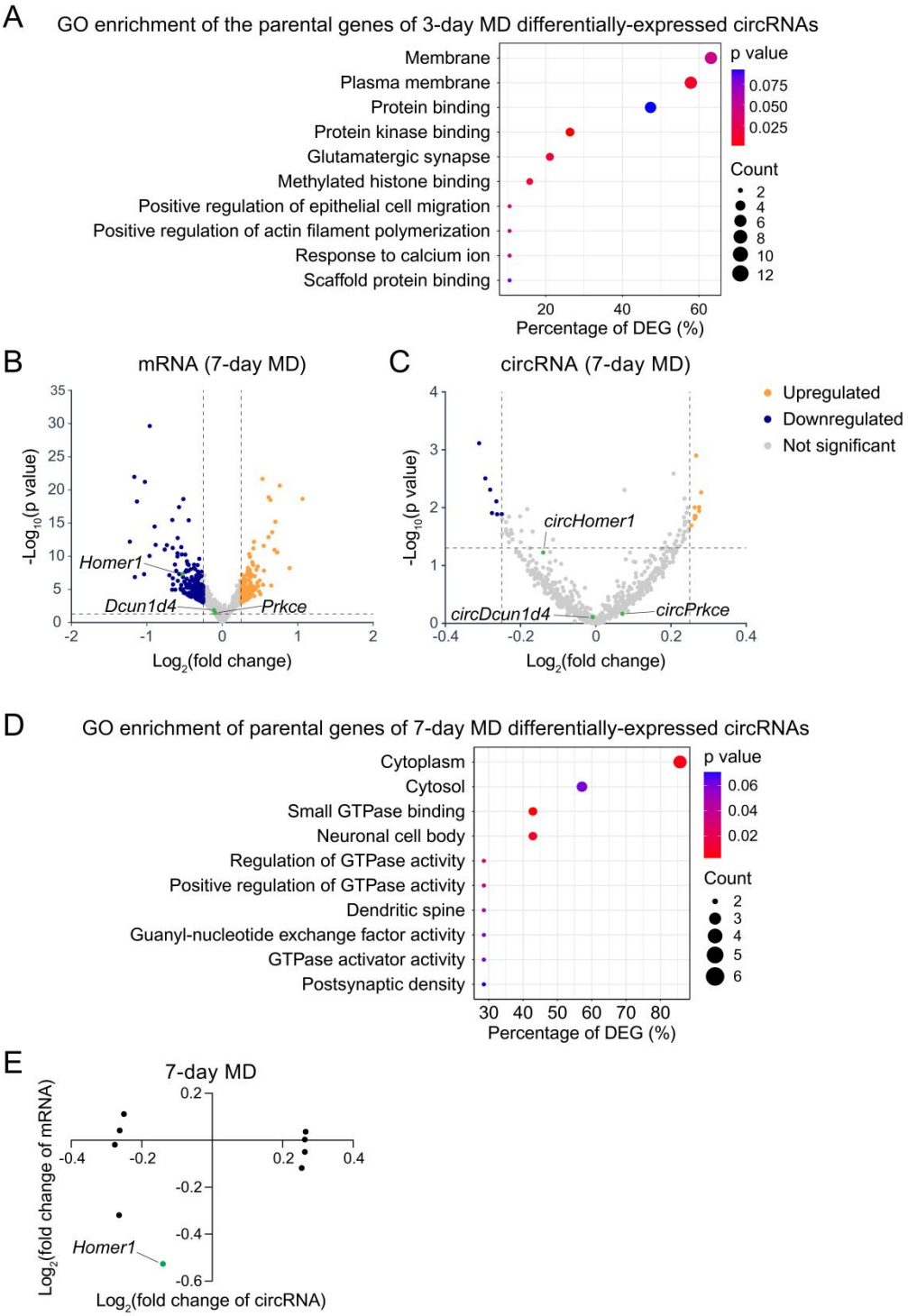

Figure S1. Transcriptomic analyses after MD in mouse V1, Related to Figure 1.

(A) GO enrichment of the parental genes of differentially-expressed circRNAs after 3-day MD. DEG, differentially-expressed gene.

(B) Volcano plot of mRNA sequencing of V1 after 7-day MD (*n* = 4 mice per group).

(C) Volcano plot of circRNA sequencing of V1 after 7-day MD (*n* = 4 mice per group).

(D) GO enrichment of the parental genes of differentially-expressed circRNAs after 7-day MD.

(E) Fold change of differentially-expressed circRNAs and their linear isoforms after 7-day MD.

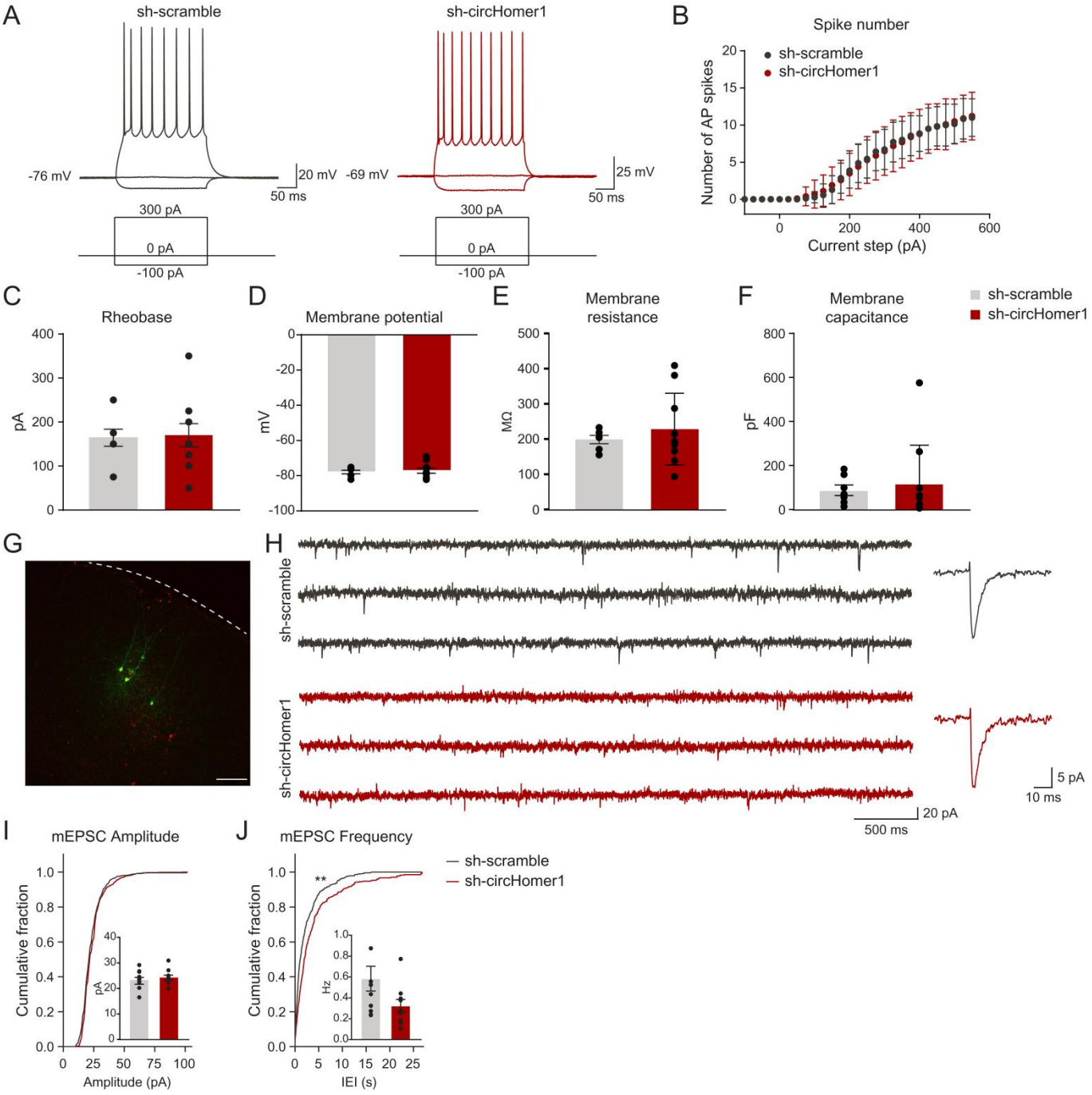

Figure S2. Characterization of the effects of *circHomer1* depletion on membrane properties and synaptic properties in layer 2/3 neurons of binocular V1, Related to Figure 4.

(A) Representative traces show the response of sh-scramble or sh-circHomer1 infected neurons to -100, 0, and 300 pA current steps. The duration of each current step was 250 ms.

(B) Quantification of the number of action potential spikes per current injection step shows the input-output relationship in sh-scramble and sh-circHomer1 infected neurons.

(C) Rheobase, defined as the minimum amount of current injected to elicit action potential firing, was measured in response to the current injection protocol (*n* = 7-10 neurons per group, Student's t-test).

(D-F) Passive membrane properties were measured in sh-scramble and sh-circHomer1 infected neurons (*n* = 7-10 neurons per group, Student's t-test).

(G) A representative image of the injection site shows an area of lentivirus-infected neurons in red, and in green three biocytin-filled cells that were recorded. The dotted line along the pial surface indicates the outline of the imaged

slice. Scale bar = 100 μm.

(H) Left, representative traces recorded from neurons in layer 2/3 of V1 expressing sh-scrambled (top) or sh-circHomer1 (bottom) lentivirus. Right, all events detected were scaled and averaged to show the average mEPSC kinetics.

(I-J) Quantification of mEPSC amplitude (I) and frequency (J) in sh-scramble or sh-circHomer1 infected neurons (n = 10 neurons per group, two-sample Kolmogorov-Smirnoff test).

Data are presented as mean ± SEM. **$p < 0.01$.

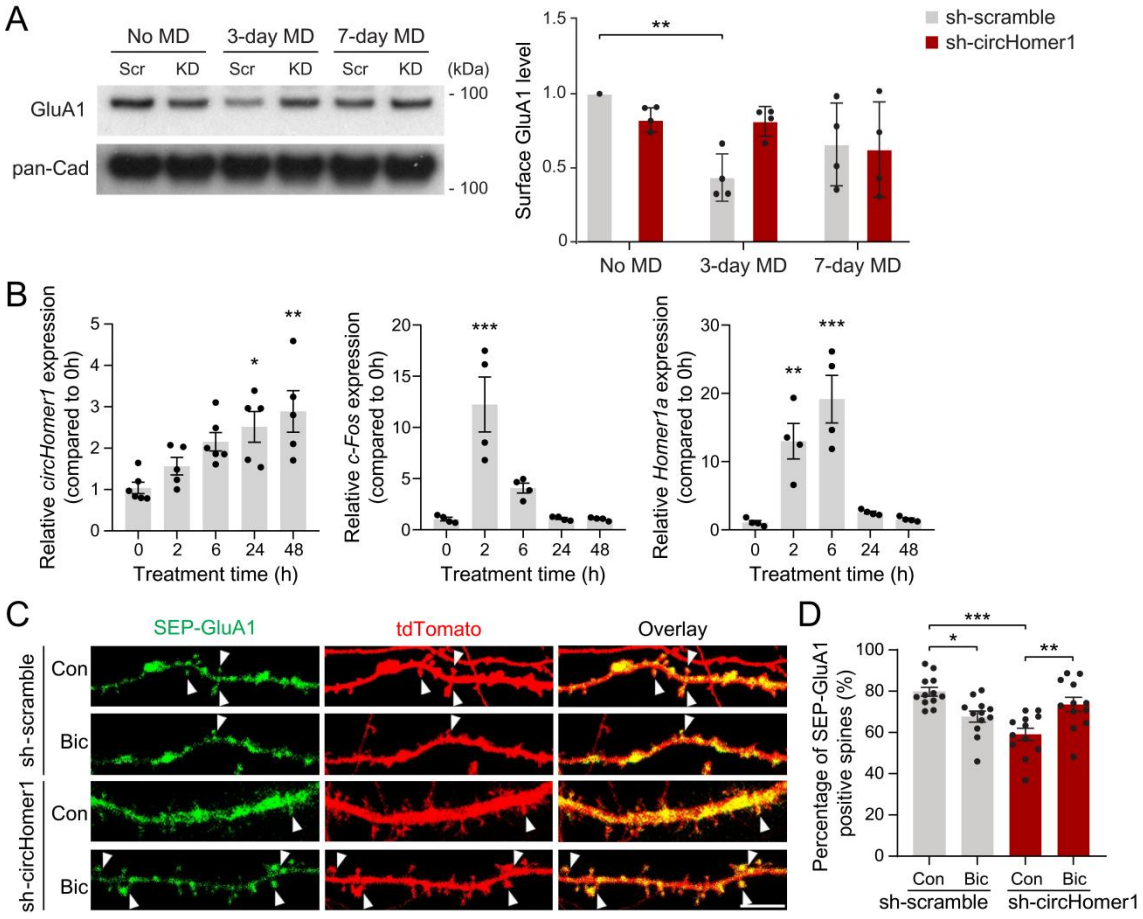

Figure S3. Alterations of surface AMPA receptor expression after *circHomer1* depletion, Related to Figure 4.

(A) Left: Western blot of cell surface expression of GluA1 in V1 of mice infected with lentivirus after MD. Scr, sh-scramble; KD, sh-circHomer1. Right: Quantification of surface GluA1 level (n = 4 mice per group, two-way ANOVA following Tukey multiple comparisons).

(B) Expression of *circHomer1* (left), *c-Fos* (middle), and *Homer1a* (right) RNAs following bicuculline treatment in cultured cortical neurons (n = 4-5 per group, one-way ANOVA following Tukey multiple comparisons).

(C) Representative images of cultured hippocampal neurons' dendrites co-transfected with SEP-GluA1 together with sh-scramble (top) or sh-circHomer1 (bottom) at DIV 11. Neurons were treated with bicuculline (20 μM) for 48 hours at DIV 17, and fixed at DIV 19. Con, control treatment; Bic, bicuculline treatment. Scale bar = 5 μm.

(D) Percentage of SEP-GluA1-positive spines under different conditions. For each neuron, 3 segments of dendrite with length of 30 μm were randomly selected, and the average percentage were calculated (n = 12 neurons per group, two-way ANOVA following Tukey multiple comparisons).

Data are presented as mean ± SEM. *p < 0.05; **p < 0.01; ***p < 0.001.

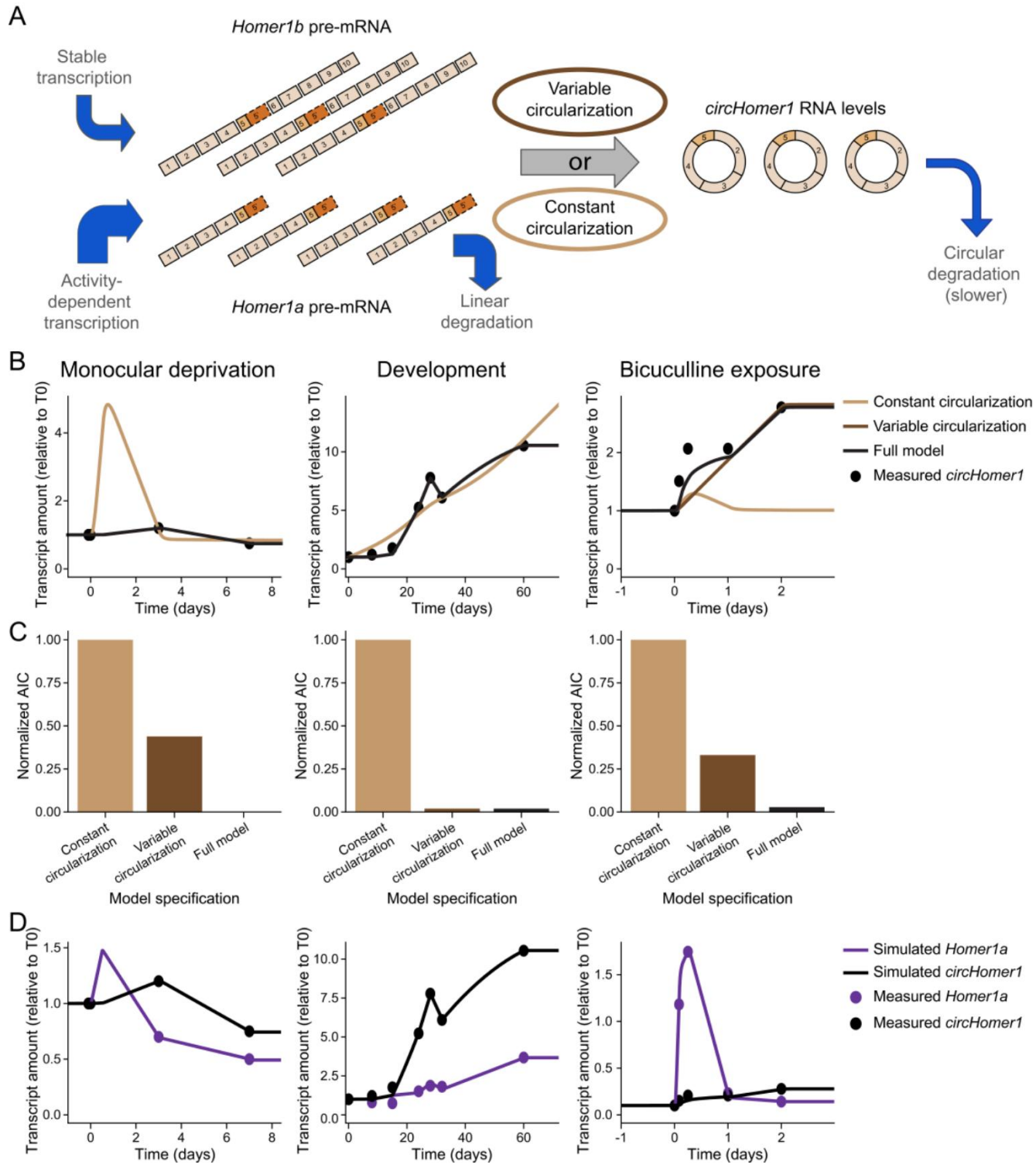

Figure S4. Modeling of *circHomer1* expression, Related to Discussion.

(A) Schematic of the model components for each experiment. Arrows represent rates fit in each model of either transcription, circularization, or degradation. These values were fit for each model and experiment combination separately to minimize squared error from measured *Homer1a* and *circHomer1* levels.

(B) Simulated levels of *circHomer1* RNA for the constant circularization (light brown), variable circularization (brown), and full models (black) for monocular deprivation (left), development (middle), and bicuculline (right) experiments. The measured, normalized levels of *circHomer1* in each experiment are overlaid (black dots).

(C) Normalized Akaike information criterion (AIC) scores for each model tested.

(D) Expanded results from the full models, showing the simulated levels of both *circHomer1* and *Homer1a* RNA (black and purple lines, respectively) overlaid with the experimentally measured levels of *circHomer1* and *Homer1a* RNA (black and purple dots, respectively) for each experiment.

Table S3. Primers list, Related to STAR Methods.

Primer	Sequence (5'-3')
Mmu_circHomer1_F	TTCCACATAGGGAGCAACC
Mmu_circHomer1_R	TCTTCTTTGTGTTCGGGTCA
Mmu_Homer1a_F	GAAGTCGCAGGAGAAGATG
Mmu_Homer1a_R	TGATTGCTGAATTGAATGTGTACC
Mmu_Bdnf_F	GACGACATCACTGGCTGACA
Mmu_Bdnf_R	CAAGTCCGCGTCCTTATGGT
Mmu_Nptx2_F	AGACAGAGAGCACGCTGAAC
Mmu_Nptx2_R	TTGAATGCACTGTTGCCTCG
Mmu_Stat1_F	AGAACGGAGGTGAACCTGAC
Mmu_Stat1_R	TCGGCAGCCATGACTTTGTA
Mmu_linear Homer1_F	ACCCGATGTGACACAGAACT
Mmu_linear Homer1_R	GTTGCTTCCACTGCTTCACA
Mmu_circTulp4_F	TCACTGTCGCAGAGATAGGAGT
Mmu_circTulp4_R	GGCACTTGATATGTTTGTTTTCC
Mmu_Gapdh_F	TCATGACCACAGTCCATGCC
Mmu_Gapdh_R	CAGATCCACGACGGACACAT
Rat_circHomer1_F	TTTCACATAGGGAACAACC
Rat_circHomer1_R	TCTTCTTTGTGTTTGGGTCG
Rat_c-fos_F	TTTCAACGCGGACTACGAGG
Rat_c-fos_R	GCGCAAAAGTCCTGTGTGTT
Rat_Homer1a_F	GAAGTCGCAGGAGAAGATG
Rat_Homer1a_R	TGATTGCTGAATTGAATGTGTACC
Rat_Gapdh_F	AGACAGCCGCATCTTCTTGT
Rat_Gapdh_R	CTTGCCGTGGGTAGAGTCAT